Review and syntheses: Ocean alkalinity enhancement and carbon dioxide removal through coastal enhanced silicate weathering with olivine

Luna J. J. Geerts[1], Astrid Hylén[1], Filip J. R. Meysman[1,2]

[1]Geobiology, Department of Biology, University of Antwerp, 2610 Wilrijk Antwerp, Belgium
[2]Department of Biotechnology, Delft University of Technology, Van der Maasweg 9, 2629 HZ Delft, The Netherlands

Correspondence: Luna J. J. Geerts (luna.geerts@uantwerpen.be)

Abstract. Coastal enhanced silicate weathering (CESW) is increasingly receiving attention as a marine-based carbon dioxide removal (CDR) technology. The method aims to achieve ocean alkalinity enhancement (OAE) by introducing fast-weathering silicate minerals into coastal systems. The latter is envisioned to act as a large natural biogeochemical reactor, where ambient physical and biological processes can stimulate silicate dissolution, thus generating a concomitant alkalinity release and increasing the seawater's capacity to sequester CO_2. Olivine has been forwarded as the prime candidate mineral for CESW, but to the present, no results from larger-scale field studies in actual coastal systems are available, so all information is exclusively derived from idealized laboratory experiments. As a result, key uncertainties remain concerning the efficiency, CO_2 sequestration potential, and impact of olivine-based CESW under relevant field conditions. In this review, we summarize recent research advancements to bridge the gap between existing laboratory results and the real-world environment in which CESW is intended to take place. To this end, we identify the key parameters that govern the dissolution kinetics of olivine in coastal sediments, and the associated CO_2 sequestration potential, which enable us to identify a number of uncertainties that are outstanding with respect to the implementation and upscaling of olivine-based CESW, as well as the monitoring, reporting, and verification (MRV). From our analysis, we conclude that the current knowledge base is not sufficient to predict the outcome of *in situ* CESW applications. Particularly, the impact of pore water saturation on the olivine dissolution rate and the question of the additionality of alkalinity generation remain critical unknowns. To more confidently assess the potential and impact of olivine-based CESW, dedicated pilot studies under filed conditions are needed, which should be conducted at a sufficiently large spatial scale and monitored for a long enough time with sufficient temporal resolution. Additionally, our analysis indicates that the specific sediment type of the application site (e.g. cohesive versus permeable) will be a critical factor for olivine-based CESW applications, as it will significantly impact the dissolution rate by influencing the ambient pore water pH, saturation dynamics, and natural alkalinity generation. Therefore, future field studies should also target different coastal sediment types.

1 Introduction

1.1 Carbon dioxide removal through ocean alkalinity enhancement

Climate stabilization is a pressing challenge for society (IPCC, 2023). Scenario analysis reveals that in addition to decarbonization, active removal of carbon dioxide (CO_2) from the atmosphere will be required to reach the targets of the COP21 Paris agreement (IPCC, 2023; Sanderson et al., 2016; UNFCCC, 2015). Such carbon dioxide removal (CDR) has to happen fast and at a sufficiently large scale: gigaton (Gt) capacity must be reached already by 2040 and this effort should increase to 12–15 Gt CO_2 yr^{-1} by 2100 (Rockström et al., 2017; Minx et al. 2018). As such, the need for technologies that can deliver such gigaton-scale CDR is high. However, research on the topic is currently still at an early stage, and so the efficiency, reliability, and environmental impact of most CDR techniques remain poorly constrained (Fuss et al., 2018; Minx et al., 2018; NASEM, 2022; Smith et al., 2016; Terlouw et al., 2021).

One proposed CDR technique is ocean alkalinity enhancement (OAE), which aims to increase the ocean's capacity to store CO_2 by raising the alkalinity level of surface waters (Hartmann et al., 2013; Renforth and Henderson, 2017). Alkalinity is the excess of proton acceptors (bases) over proton donors (acids) in solution and governs the CO_2 storage capacity of seawater (Dickson, 1984; Zeebe and Wolf-Gladrow, 2001). The addition of alkalinity shifts the reaction equilibria of the carbonate system from dissolved CO_2 towards bicarbonate (HCO_3^-) and carbonate (CO_3^{2-}), thus allowing more atmospheric CO_2 to dissolve in the seawater (Wolf-Gladrow et al., 2007). Compared to other CDR approaches, OAE has the advantage that the CO_2 sequestration potential is considered to be substantial (0.1–1 Gt CO_2 yr^{-1}) and that CO_2 storage is essentially permanent over a time scale of thousands of years (Caserini et al., 2022; Meysman and Montserrat, 2017; NASEM, 2022; Renforth and Henderson, 2017). OAE is also the natural way by which the Earth system has responded in the geological past to neutralize natural CO_2 additions to the atmosphere and counteract global warning (Archer et al., 2009) (Fig. 1a). This nature-based character of OAE could help increase the societal acceptance of the CDR method (Corner and Pidgeon, 2015). Moreover, OAE has the important benefit of counteracting ocean acidification, which is not the case for CDR techniques that target organic carbon sequestration (Campbell et al., 2022; Caserini et al., 2022; Meysman and Montserrat, 2017).

The crux of any OAE technique relates to the source of the alkalinity that is added to the surface ocean, and several different OAE approaches have been suggested (Fig. 1b) (NASEM, 2022). "Fast-addition OAE approaches" aim to introduce alkalinity directly to surface waters, and the alkalinity is generated either by electrochemical methods (generation of base, such as NaOH, through electrolysis of seawater) or by ocean liming (addition of nearly instantly dissolving basic minerals, such as Ca(OH)$_2$ or Mg(OH)$_2$) (Campbell et al., 2022; Caserini et al., 2022; Renforth and Henderson, 2017). These technologically-oriented methods require the construction of large reactor infrastructure to produce the alkaline products that enable OAE (electrolyzer plants, lime kilns), thus necessitating substantial capital investments (NASEM, 2022; Rau, 2008; Renforth et al., 2013). These approaches also need high amounts of energy per ton of CO_2 sequestered (electrochemistry) or require the installment of additional carbon capture capacity (CO_2 capture during lime production). In contrast, "slow-addition OAE approaches" are based on chemical mineral weathering, and are "nature-inspired" in the sense that they aim to mimic a natural process of

alkalinity generation. The idea underlying enhanced weathering (EW) approaches is to add specific mineral types to coastal and shelf sediments, which then gradually dissolve over a time scale of years to centuries, thus gradually releasing alkalinity from the seabed to the overlying water (Campbell et al., 2022; Hartmann et al., 2013; NASEM, 2022). The production of

65 rapidly weathering minerals and their addition to the seafloor requires far less energy than technology-oriented approaches, as it capitalizes on natural energy sources, such as the exergonic nature of the dissolution reaction and the *in situ* "milling" of particles using energy from waves and currents (Meysman and Montserrat, 2017; NASEM, 2022). Moreover, no large reactor infrastructure is needed, as one essentially uses the coastal system as the biogeochemical reactor. As such, the method offers the prospect of rapid scalability, as it can be integrated within current marine engineering practices (e.g. beach nourishment,

70 dredging, land reclamation) using existing technology and infrastructure (ports, ships, dredging equipment) (Meysman and Montserrat, 2017). A range of minerals have been considered as source material for EW-based OAE, including naturally occurring silicates (Huijgen et al., 2006; Lackner, 2002; te Pas et al., 2023) and carbonates (Harvey, 2008), but also waste and overburden material (Bullock et al., 2021; Renforth, 2019; Vandeginste et al., 2024). However, the most attention has so far been devoted to the silicate mineral olivine, which is characterized by a fast intrinsic weathering rate. In this review, we

75 synthesize the current knowledge on coastal enhanced silicate weathering (CESW) using olivine as a way to achieve OAE.
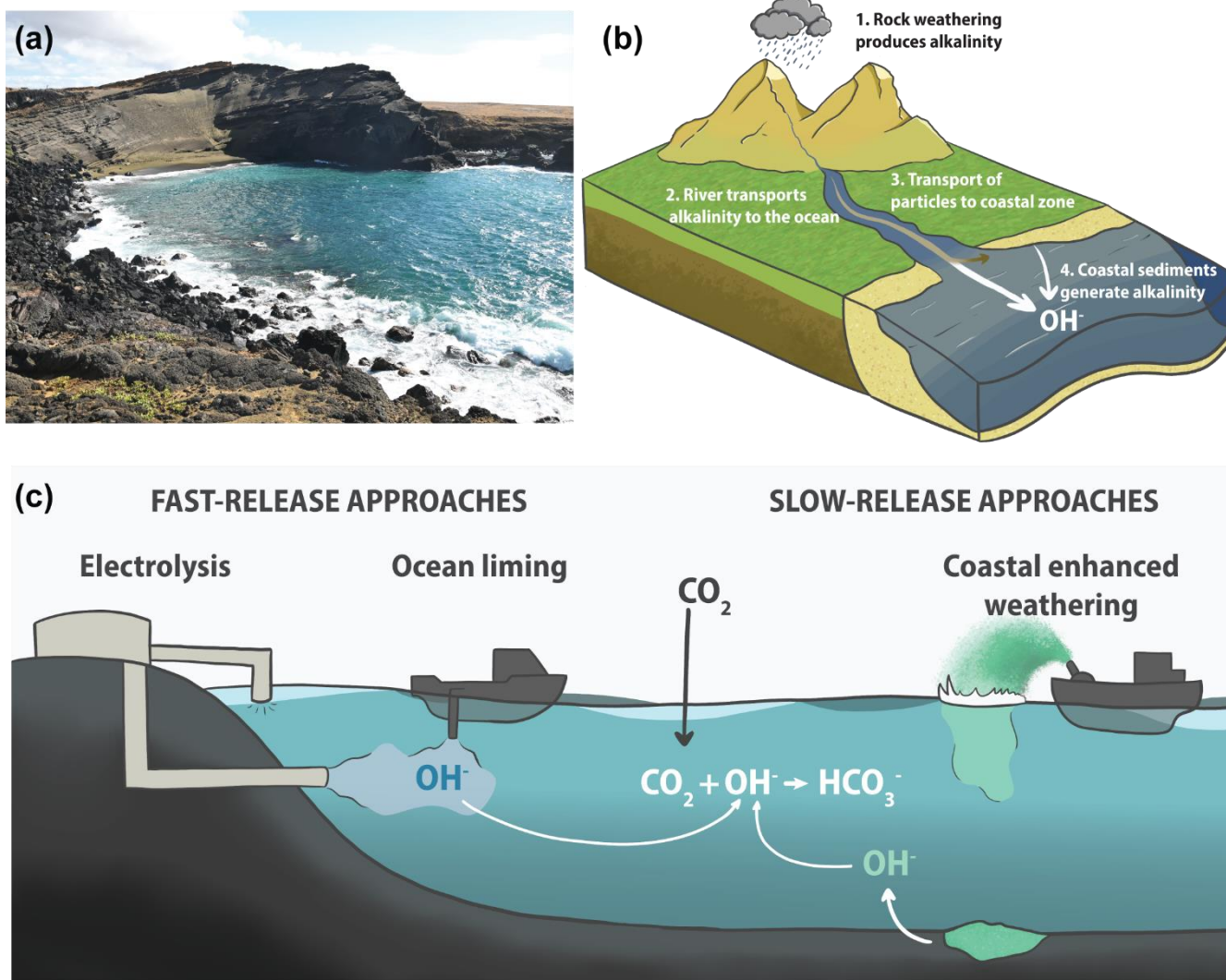
Figure 1. Ocean alkalinity enhancement. (a) An example of a location with natural coastal ocean alkalinity enhancement. Papakōlea Beach in Hawaii is one of the few locations where olivine sand is naturally present at Earth's surface. (b) General scheme of natural ocean alkalinity enhancement. Chemical weathering on land produces mineral particles and dissolved products, including alkalinity (here depicted as OH⁻). Minerals and alkalinity are transported by rivers to the ocean. Mineral particles are deposited in coastal sediments, chemically weather, and generate additional alkalinity. (c) Anthropogenic ocean alkalinity enhancement. During fast-release approaches, alkalinity is directly introduced into the ocean by electrolysis of seawater (which creates NaOH) or through ocean liming (addition of nearly instantly dissolving basic minerals, such as $Ca(OH)_2$ or $Mg(OH)_2$). During slow-release approaches, minerals (e.g., olivine) are applied to the seafloor, and alkalinity is slowly released via chemical weathering.

1.2 Ocean alkalinity enhancement via coastal enhanced silicate weathering

The proof of the principle that silicate weathering can draw down atmospheric CO_2 is embedded in Earth's geological record. Rising temperatures and a higher acidity of natural waters resulting from higher CO_2 concentrations increase the weathering rate of silicate rocks (Berner, 2004; Berner et al., 1983). The chemical dissolution of silicate minerals in terrestrial and coastal

environments releases alkalinity into the surface ocean (Fig. 1b), where it drives the uptake of CO_2 from the atmosphere

90 (Hartmann et al., 2013; Schuiling and Krijgsman, 2006). This negative feedback in the global carbon cycle counteracts global warming and stabilizes Earth's climate over a time scale of thousands of years (Berner, 2004; Berner et al., 1983; Raymo and Ruddiman, 1992). Note that silicate weathering will eventually also neutralize the CO_2 that is released from current anthropogenic activities (Archer et al., 2009). However, the timescale of this response is too slow (> 10,000 years) for society, as it implies that we have to "sit through" an extended period of global warming before the anthropogenic CO_2 is removed

95 naturally. The ultimate aim of CESW is to accelerate the silicate weathering feedback, reducing the timescale of response from millennia down to decennia.

The idea underlying CESW is to selectively use (ultra)mafic source rocks that are enriched in silicate minerals with high dissolution rates (e.g. olivine), pulverize the source rock into small particles to increase the reactive surface area, and distribute the mineral particles in coastal and shelf environments with high weathering potential (Fig. 2) (Meysman and Montserrat,

100 2017; Schuiling and Krijgsman, 2006). Three different CESW application scenarios have been proposed depending on the target sediment type and application location within the coastal and shelf zone (Meysman and Montserrat, 2017). In the *bedload scenario* (Fig. 2b), silicate sand is deposited in areas with high hydrodynamic energy (e.g. gravel or rock beds) to promote further physical grinding of the silicate grains during bedload transport (Meysman and Montserrat, 2017; Schuiling and Krijgsman, 2006). In this scenario, minerals remain in close contact with the overlying seawater, and the weathering primarily

105 takes place on top of the seafloor. In the *permeable sediment scenario* (Fig. 2c), silicate sand is mixed into permeable sediments characterized by high advective flows. The advective flushing prevents the build-up of dissolution products in the sediment, which could otherwise slow down the silicate dissolution rate and cause precipitation of secondary minerals (Meysman and Montserrat, 2017). In the *cohesive sediment scenario* (Fig. 2d), fine silicate particles are mixed into impermeable, fine-grained sediments where biotic processes can enhance dissolution. Bioirrigation flushes the sediment, removing dissolution products and supplying O_2 to deeper sediment layers (Meysman et al., 2007). Oxic mineralization of organic matter, reoxidation of

110 reduced compounds, and the activity of certain microbes (e.g. cable bacteria, Meysman, 2018; Pfeffer et al., 2012) decrease the sedimentary pH and thereby could enhance the silicate dissolution (Rao et al., 2014; Rimstidt et al., 2012; Silburn et al., 2017; Wallmann et al., 2008; Widdicombe et al., 2011). Macrofauna could also speed up the dissolution of silicate minerals through ingestion due to high enzymatic activity and low pH in the guts, combined with mechanical abrasion (Meysman and

115 Montserrat, 2017). The physical and biological mechanisms that can stimulate the dissolution of silicate minerals in coastal and shelf sediments have collectively been referred to as the "benthic weathering engine" (Meysman and Montserrat, 2017). As further detailed below, very little *in situ* data on the strength and efficiency of the different processes contributing to this benthic weathering engine are yet available. As a result, it is unclear which of the three scenarios (and hence which type of sediment locations) is the most promising for CESW.

120
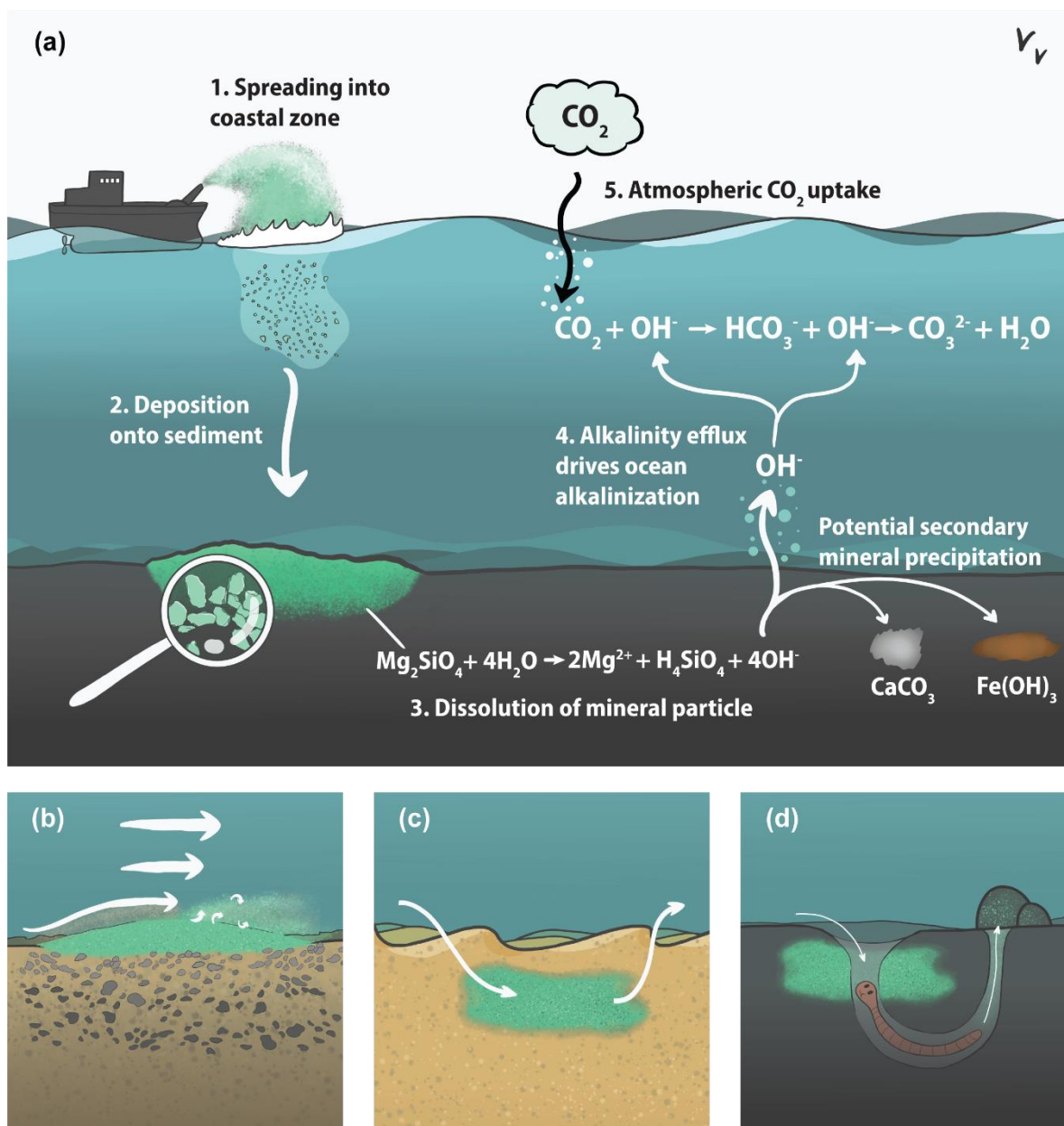
Figure 2. Principle of coastal enhanced silicate weathering (CESW) as a method for ocean alkalinity enhancement, including suggested application scenarios (Meysman and Montserrat, 2017). (a) Schematic overview of CESW: (1) Finely ground particles of a fast-weathering silicate mineral (e.g. olivine) are spread in the coastal zone. (2) The silicate minerals are deposited onto or mixed into the sediment. (3) The silicate minerals dissolve, releasing alkalinity (here depicted as OH⁻) to the pore water. (4) Alkalinity is

125 **either transported from the sediment to the overlying water, leading to ocean alkalinity enhancement or is trapped in the sediment by secondary reactions. (5) Upon alkalinity addition, the seawater carbonate system re-equilibrates with the atmosphere, leading to an uptake of CO_2. (b) Bedload application scenario. Silicate minerals are deposited on top of the sediment, allowing bedload transport to naturally grind the grains to smaller sizes. (c) Permeable sediment application. High advective flows flushing the pore water and preventing the buildup of weathering products. (d) Cohesive sediment application. Bioirrigation leads to flushing of the**

1.3 Scope of this review

This review focuses on CESW using olivine, which is the mineral that has been given the most attention due to its relatively fast dissolution rate (four orders of magnitude faster than quartz) combined with a relatively widespread abundance

135 (commercial mines are operating across the globe) (Harben and Smith, 2006; Hartmann et al., 2013). In recent years, the CESW literature has discussed various aspects of enhanced olivine weathering, such as rock grinding requirements (Hangx and Spiers, 2009; Strefler et al., 2018), application areas and CO_2 sequestration efficiency (Bertagni and Porporato, 2022; Köhler et al., 2010; Moosdorf et al., 2014), life cycle analysis (Foteinis et al., 2023), secondary precipitation and dissolution reactions (Flipkens et al., 2023b; Fuhr et al., 2022; Montserrat et al., 2017; Rigopoulos et al., 2018), and olivine dissolution

140 rates (Hangx and Spiers, 2009; Heřmanská et al., 2022; Oelkers et al., 2018; Rimstidt et al., 2012). No data is yet available from mesocosm experiments or large-scale *in situ* pilots. While the first mesocosm experiments and field trials are currently being planned or are in the first stage of execution (e.g., Vesta, 2023), no publications or reports have yet emerged on their outcomes. Therefore, the information currently available on CESW is either deduced from laboratory-scale dissolution experiments or based on modeling. Begging the question to what extent these results can be confidently extrapolated to a real-

145 world application. Dissolution experiments are typically performed under idealized conditions with high fluid-to-mineral ratios, which is the opposite of natural sediments. Several studies have investigated olivine dissolution in artificial seawater (Fuhr et al., 2022; Montserrat et al., 2017; Rigopoulos et al., 2018), while fewer studies have used natural seawater (Flipkens et al., 2023b; Montserrat et al., 2017), and only two studies include sediment (Bach, 2024; Fuhr et al., 2023). Furthermore, while small-scale experiments in benchtop reactors or microcosms are key to constraining specific parameters and attaining

150 detailed process knowledge, they do not replicate the physical and biological transport and biogeochemical reactions within the natural seafloor. Therefore, a critical challenge for olivine-based CESW is the lack of information obtained from suitably large-scale experiments that are performed under *in situ* conditions, which is essential for assessing its real-world applicability (Cyronak et al., 2023; Meysman and Montserrat, 2017; Renforth and Henderson, 2017; Riebesell et al., 2023). Consequently, critical questions remain regarding the feasibility, efficiency, and ecosystem impacts of olivine-based CESW.

155 In this review, we summarize recent research advancements seen through the lens of practical implementation of olivine-based CESW. Compared to previous reviews on CESW (Vandeginste et al., 2024; Wang et al., 2023), we concentrate on the context of coastal sediments since the conditions within this application environment are central to the outcome of CESW. Our focus is on predictability: given a target site in the coastal ocean, how confidently can we predict the olivine dissolution rate and the associated rate of alkalinity release and CO_2 sequestration? What aspects and parameters need consideration, and which are

160 currently uncertain (Table 1)? What aspects need specific consideration when performing future mesocosm pilots and field trials? Compared to previous work on CESW, we specifically consider the heterogeneity of sediments within the coastal ocean and hence the impact of sediment texture. We direct our attention to the various parameters that determine mineral dissolution rates in different types of coastal sediments and we evaluate the ensuing CO_2 sequestration during olivine-based CESW. Our

goal is to bridge the gap between the experimental laboratory studies that have been conducted so far and the real-world
165 environment. We review the importance of processes that could hamper the efficiency of CESW (e.g., cation-depleted surface layers, secondary mineral formation, pore water saturation) and highlight aspects that demand further scrutiny in future experiments and field trials. Finally, we discuss some issues relevant to efficient monitoring, reporting, and verification (MRV) of CESW applications.

170 **Table 1 Overview of parameters and terminology used in the manuscript.**

Symbol	Parameter	Value
A_0	Pre-exponential factor Arrhenius equation (mol m^{-2} s^{-1})	
A_{BET}	BET measured specific surface area (m^2 g^{-1})	
A_{geo}	Geometric specific surface area (m^2 g^{-1})	
A_{surf}	Specific surface area (m^2 g^{-1})	2–8
a_{H_2O}	Water activity (unitless)	
$C_{mineral}$	Mineral content of sediment at a given time (g mineral m^{-2} seafloor)	
D_e	Equivalent grain diameter (m)	
D_{max}	Maximum grain size in grain size interval (m)	
D_{min}	Minimum grain size in grain size interval (m)	
E_a	Activation energy of olivine dissolution in Arrhenius equation (kJ mol^{-1})	70.4 (pH < 5.6), 60.9 pH > 5.6 [1]
k_d	Intrinsic dissolution rate constant of olivine (mol m^{-2} s^{-1})	
$L_{mineral}$	Mineral loadning, $C_{mineral}$ at t_0 (g mineral m^{-2} seafloor)	
M_{CO_2}	Molar mass of CO_2 (g mol^{-1})	44.01
M_{FAY}	Molar mass of fayalite (g mol^{-1})	203.77[2,3]
M_{FOR}	Molar mass of forsterite (g mol^{-1})	140.69[2,3]
$M_{olivine}$	Molar mass of olivine (g mol^{-1})	140.69–203.77[2,3]
P_{CO_2}	CO_2 capture potential (g CO_2 sequestered g^{-1} dissolved olivine)	
R	Universal gas constant (kJ K^{-1} mol^{-1})	8.314 x 10^{-3}
$F_{mineral}$	Areal mineral weathering rate (g mineral dissolved m^{-2} seafloor yr^{-1})	
F_{A_T}	Areal alkalinity release rate (mol alkalinity m^{-2} seafloor yr^{-1})	
F_{CO2}	Areal CO_2 sequestration rate (g CO_2 m^{-2} seafloor yr^{-1})	
R_{diss}	Specific mineral dissolution rate (g mineral dissolved g^{-1} mineral present yr^{-1})	
R_S	Grain roughness (unitless)	2–8
T	Temperature (K, C°)	
$V_{olivine}$	Molar volume of olivine (m^3 mol^{-1})	4.365×10^{-5}[2]

x_{FAY}	Mole fraction fayalite in olivine (unitless)	0.07–0.20
x_{inert}	Mass fraction inert minerals in dunite source rock (unitless)	0–0.1
γ_{A_T}	Alkalinity production factor (mol alkalinity released mol^{-1} olivine dissolved)	0–4
μ_{SR}	Alkalinity scavenging by secondary reaction factor (unitless)	0–1
ρ_{CO_2}	CO_2 sequestration efficiency (mol CO_2 mol^{-1} alkalinity)	0.75–0.90[4,5]
φ	Fraction forsterite in particular grain diameter class	
Ω	Saturation index of mineral dissolution reaction (unitless)	0–1

[1](Rimstidt et al., 2012), [2](Deer et al., 2013), [3](Flipkens et al., 2021), [4](Bertagni and Porporato, 2022), [5](Schulz et al., 2023)

2 Olivine rocks and their availability

2.1 Olivine composition and dissolution

Olivine ($Mg_{(2-x)}Fe_xSiO_4$) constitutes a common group of igneous minerals, with compositions ranging from the magnesium
175 endmember forsterite (Mg_2SiO_4, M_{FOR} = 140.69 g mol^{-1}) to the iron endmember fayalite (Fe_2SiO_4, M_{FAY} = 203.77 g mol^{-1})
(Deer et al., 2013; Kremer et al., 2019). The molar mass of olivine ($M_{olivine}$) hence reflects the ratio between forsterite and
fayalite, with $M_{oli} = (1-x_{FAY})M_{FOR} + x_{FAY}M_{FAY}$, where x is the molar fraction of fayalite. Olivine also contains the trace
metals nickel (Ni) and chromium (Cr). Ni substitutes the divalent cations in olivine (Mg^{2+}, Fe^{2+}), and its content ranges from
0.2–1.2 mol% (Keefner et al., 2011; Montserrat et al., 2017; Santos et al., 2015). Cr is typically present as chromite ($FeCr_2O_4$)
180 inclusions at lower concentrations of 0.02–0.66 mol% (Deer et al., 2013; Flipkens et al., 2021). The fate of these metals upon
dissolution and their potential impact on marine ecosystems remains an important topic of research for CESW (Bach et al.,
2019; Flipkens et al., 2021, 2023a; Foteinis et al., 2023), but falls outside of the scope of this review.

Olivine is one of the most rapidly weathering silicate minerals (Table 2) due to its structure, which consists of independent
silicate tetrahedra (SiO_4) linked by relatively weak Mg/Fe-O bonds (Sun and Huggins, 1947). This structure differs from most
185 other silicate minerals, in which SiO_4 tetrahedra are connected through a Si-O-Si bond, which has a three times greater bond
strength and hence is much harder to break (Velbel, 1999). Once the metal ion (Mg^{2+}/Fe^{2+}) in olivine is mobilized, the SiO_4
tetrahedra are also liberated and move into solution as dissolved orthosilicic acid, $Si(OH)_4$ (Oelkers et al., 2018). Note that a
few other silicate minerals have dissolution rates that are comparable to or even higher than forsterite (Table 2), including
wollastonite ($CaSiO_3$; Lackner, 2002; Huijgen et al., 2006) and anorthite ($CaAl_2Si_2O$; te Pas et al., 2023). However, these
190 minerals have received less attention for CESW, as they are not as abundant as olivine, but also because their CO_2 capture
potential is not as high as that of forsterite. Per gram of dissolved mineral, forsterite can ideally capture 1.25 g of CO_2, while
the corresponding values are 0.76 g CO_2 for wollastonite, 0.32 g CO_2 for anorthite, and 0.17 g CO_2 for albite (te Pas et al.,
2023). Carbonates (calcite, dolomite) also dissolve faster than olivine and do not contain trace metals, making them interesting
minerals for coastal enhanced weathering (Bach, 2024; te Pas et al., 2023). However, carbonates bear the risk of pore water

195 oversaturation and re-precipitation, thus strongly reducing the efficiency of CO_2 sequestration (Bach, 2024; Hartmann et al., 2013).

Table 2. Dissolution times of different minerals, assuming a 1 mm radius sphere dissolving in water at pH 5 and a temperature of 25°C. Adapted from Lasaga et al. (1994) and Hartmann et al. (2013). ªThe molar volume of albite is greater than that of serpentine, giving the minerals different dissolution times for the same reactivity.

Mineral	Reactivity (log mol m^{-2} s^{-1})	Dissolution time (years)
Quartz[1]	-13.39	34,000,000
Kaolinite[1]	-13.28	6,000,000
Muscovite[1]	-13.07	2,600,000
Epidote[1]	-12.61	923,000
Albite[a, 1]	-12.26	575,000
Serpentine[a, 2]	-12.26	533,000
Sepiolite[3]	-11.85	79,000
Enstatite[1]	-10.00	10,100
Diopside[1]	-10.15	6,800
Forsterite[4]	**-9.36**	**1680**
Anorthite[1]	-8.55	112
Wollastonite [1]	-8.00	79
Dolomite[5]	-17.82	1.6
Calcite[5]	-19.04	0.1

[1](Lasaga et al., 1994), [2](Orlando et al., 2011), [3](Mulders et al., 2018), [4](Rimstidt et al., 2012), [5](White and Brantley, 1995)

2.2 Olivine source rocks

Olivine is a major constituent of many ultramafic and mafic igneous rocks such as gabbro, peridotite, and basalt, where it coexists with plagioclase and pyroxene (Deer et al., 2013; Klein et al., 2002). Because olivine is so easily altered by weathering,

205 it is not commonly found at the Earth's surface (Delvigne et al., 1979; Wilson, 2004). The highest concentration of olivine is found in peridotite, which is an umbrella term for ultramafic rocks containing at least 40 weight% olivine (Fig. 3a). Peridotite is further divided into dunite, harzburgite, wehrlite, and lherzolite, based on the relative abundance of olivine relative to orthopyroxene and clinopyroxene (Fig. 3a). Dunite contains over 90 weight% olivine by definition, and is, therefore, the most relevant peridotite rock for CESW (Caserini et al., 2022; Deer et al., 2013; Le Maitre et al., 2002). When using dunite as the

210 olivine source rock, the mass fraction of inert minerals (x_{inert}) thus ranges between 0 and 0.10.

Dunite rocks with a high forsterite content are preferred for CESW. The ferrous iron (Fe^{2+}) produced when fayalite dissolves, will precipitate back as iron (Fe^{3+}) (hydr)oxides upon contact with O_2, which consumes any alkalinity produced during fayalite dissolution (Griffioen, (2017), section 3.3.2). Therefore, fayalite does not contribute to CO_2 drawdown. Typically, the forsterite fraction of olivine is substantially higher than the fayalite fraction, with x_{FOR} values of 0.80–0.88 in Fe-rich dunites and 0.88–

215 0.94 in Mg-rich dunites, respectively (Ackerman et al., 2009; Deer et al., 2013; Harben and Smith, 2006; Rehfeldt et al., 2007; Su et al., 2016).

2.3 Availability of olivine

Olivine deposits are typically found at ultramafic intrusions (e.g. Norway, Germany), ophiolite complexes (e.g. Greece, Italy, Turkey), alpine peridotites emplaced along thrust faults (e.g. Italy, Spain), rift zones/ basalts of mid-ocean ridges (e.g. Iceland),
220 and volcanic xenoliths (e.g.German Eifel and Kaiserstuhl, Iceland) (Harben and Smith, 2006; Kremer et al., 2019) (Fig. 3b–3c). Large dunite reserves are found within the Fjordane Complex, Norway (>2 Gt), the Piedmont region in Italy (650 Mt), Horoman Hill in Japan (100 Mt), and the Xixia and Yubian Counties in China (9 Mt) (Caserini et al., 2022; Harben and Smith, 2006). In the United States, a large dunite deposit (200 Gt) is present at Twin Sister Mountain (Caserini et al., 2022; Goff et al., 2000; Kremer et al., 2019), and a smaller one (300 Mt) in North Carolina (Caserini et al., 2022; Goff and Lackner, 1998).
225 Dunite deposits are commercially exploited at several locations across the globe, as olivine is used as a slag conditioner in steel production to improve the performance and lifespan of the steel melting furnace (Harben and Smith, 2006). Established mining reserves for dunite amount to a few tens of gigatonnes (Gt), while potential resources are estimated at a few hundreds of Gt (see supplementary file 3, Harben and Smith (2006), and Caserini et al. (2022)). For reference, the global reserves for wollastonite have been estimated at ~500 Mt, with purities of 40–96 weight% (Robinson et al., 2006), and are hence
230 considerably smaller than those of olivine. At a theoretical CO_2 capture potential of 1.25 g CO_2 per g of forsterite dissolved (Hartmann et al., 2013), the currently exploited dunite reserves translate to a total CDR capacity of >50 Gt CO_2, which can increase up to a few hundred Gt if new mining deposits are exploited. The CDR potential for olivine could thus be considerable but note that the total CDR requirement over the 21st century to reach the Paris agreement targets is estimated at 400–1000 Gt CO_2 (Minx et al., 2018; Riahi et al., 2021; Rockström et al., 2017), which underlines to the extraordinary scale of the climate
235 challenge. Therefore, olivine-based CESW should be considered within a portfolio of parallel CDR approaches. The global production rate of olivine sand is currently ~8 Mt per year (Harben and Smith, 2006), so this production rate would have to increase substantially to enable large-scale CESW.

A cost-effective option for obtaining olivine sand for CESW applications would be directly extracting it from olivine-rich beaches. However, this is not a viable option, as beach resources are minimal due to the high weathering rate of olivine at
240 Earth's surface. Olivine beaches are found close to recently exposed source rock, which only occurs in a few natural coastal environments (e.g. Papakōlea beach in Hawaii, Tremblet beach in La Reunion). Moreover, some olivine beaches serve as tourist attractions or are considered sacred sites (e.g., Papakōlea beach in Hawaii), which precludes commercial sand extraction.
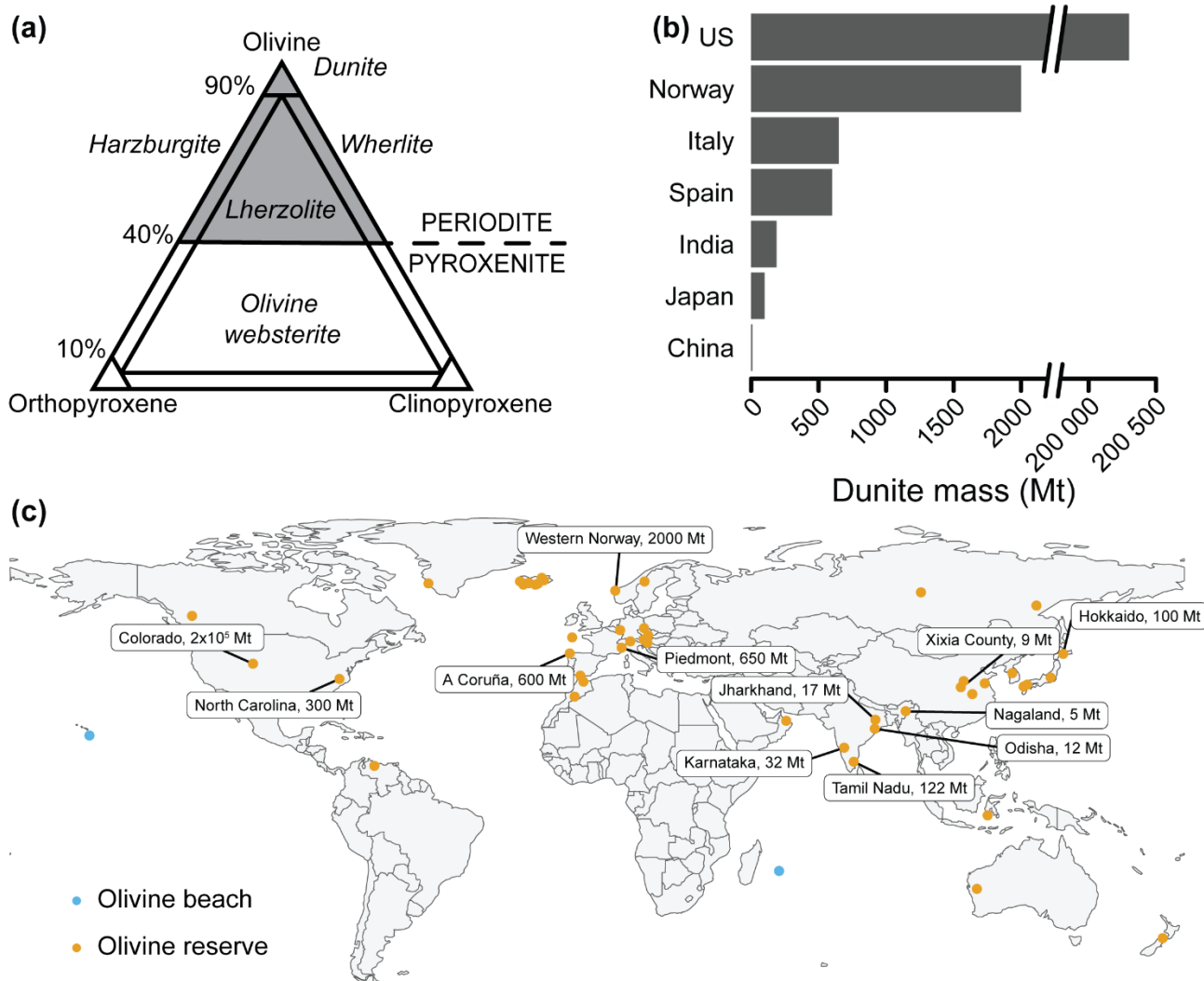
Figure 3. Olivine classification and occurrence around the globe. (a) Ternary plot for rock composed of olivine, orthopyroxene, and clinopyroxene. The peridotite group (grey) contains at least 40 weight% olivine. Dunite contains at least 90 weight% olivine. **(b)** The seven countries with the largest known dunite reserves. The best available reservoir estimate is given; the precise amount is uncertain. **(c)** Global map of locations with known dunite deposits (orange) and natural olivine beaches (blue). When known, the size of the deposit is displayed. A list of references and details is found in supplementary file 3.

3 Factors affecting the CO₂ sequestration rate during CESW

The entire process of CESW can be quantitatively described as a five-step process (Fig. 2a): (1) production of olivine sand from source rock (2) spreading and deposition onto the seabed (3) mineral dissolution, (4) alkalinity release to the overlying

water, and (5) CO₂ sequestration at the air-sea interface. In the dissolution step, the olivine sand deposited during CESW will react on top of or within the seabed. The areal weathering rate (g mineral dissolved m⁻² seafloor per unit of time) is provided

255 by the rate expression (Meysman and Montserrat, 2017):

$$F_{\text{mineral}}(t) = -R_{\text{diss}}(t)C_{\text{mineral}}(t)$$

(1)

The specific mineral dissolution rate R_{diss} denotes the amount of source mineral that is lost per unit of time (g mineral dissolved yr⁻¹ g⁻¹ mineral present), while the mineral content C_{mineral} represents the amount of olivine sand that is present per unit of application area at a given time t (g mineral m⁻² seafloor). The mineral loading $L_{\text{mineral}} = C_{\text{mineral}}(t_0)$ represents the

260 amount of olivine sand initially deposited.

This weathering process will generate a certain amount of alkalinity (A$_T$) that escapes across the sediment-water interface towards the overlying seawater. The areal alkalinity release rate (mol alkalinity m⁻² seafloor per unit of time) is linked to the areal weathering rate by:

$$F_{A_T} = \gamma_{A_T} \cdot \left(1 - \mu_{\text{SR}}\right)\left(-\frac{1}{M_{\text{olivine}}} \cdot \left(1 - x_{\text{inert}}\right) \cdot F_{\text{mineral}}\right)$$

(2)

265 The stoichiometric alkalinity production factor γ_{A_T} (mol alkalinity mol⁻¹ mineral dissolved) denotes how much alkalinity is produced upon mineral dissolution. This factor depends on the mineral at hand (e.g. olivine versus wollastonite) and the mechanism of dissolution (different end products of olivine weathering are possible, section 3.2). The factor x_{inert} represents the mass fraction of inert minerals in the source rock, i.e., accessory minerals that do not dissolve and generate alkalinity, while M_{olivine} denotes the molar mass of olivine. The quantity μ_{SR} represents the fraction of alkalinity produced during initial

270 dissolution, but which is subsequently scavenged during secondary reactions within the sediment (section 3.3). The areal alkalinity release rate F_{A_T} thus represents the alkalinity that effectively reaches the overlying water.

In the final step, CO₂ sequestration will occur at the air-sea interface. The areal CO₂ uptake rate (g CO₂ m⁻² seafloor per unit of time) can be described as:

$$F_{CO_2} = M_{CO_2} \cdot \rho_{CO_2} \cdot F_{A_T}$$

275 Here, M_{CO_2} represents the molar mass of CO₂ (44.01 g mol⁻¹), and ρ_{CO_2} denotes CO₂ sequestration efficiency, i.e., the amount of CO₂ sequestered upon adding one mole of alkalinity to seawater (mol CO₂ mol⁻¹ alkalinity). By combining Eq. 1–3, the CO₂ uptake rate can be expressed as:

$$F_{CO_2} = P_{CO_2}(t)R_{\text{diss}}(t)C_{\text{mineral}}(t)$$

(3)

The CO₂ capture potential P_{CO_2} (g CO₂ captured g⁻¹ weathered mineral sand) specifies the mass of CO₂ sequestered from the

280 atmosphere per unit mass of source rock dissolved and is formally defined as (Meysman and Montserrat, 2017):

$$P_{CO_2} = \frac{M_{CO_2}}{M_{\text{olivine}}} \cdot \rho_{CO_2} \cdot \gamma_{A_T} \cdot \left(1 - x_{\text{inert}}\right) \cdot \left(1 - \mu_{\text{SR}}\right)$$

(4)

In the following sections, we will systematically review all the parameters that control the CO_2 capture potential P_{CO_2} and mineral dissolution rate R_{diss}. All parameters are expressed for olivine-based CESW (summarized in Table 1).

3.1 Olivine dissolution rate

285 The olivine dissolution rate $R_{\mathrm{diss}}(t)$ can be parameterized as:

$$R_{\mathrm{diss}}(t) = k_{\mathrm{d}} \cdot A_{\mathrm{surf}}(t) \cdot M_{\mathrm{olivine}} \cdot (1 - \Omega(t)) \qquad (5)$$

Here, k_{d} is the intrinsic dissolution rate constant (mol olivine dissolved yr^{-1} m^{-2} of olivine surface area), A_{surf} is the specific surface area at a given time (m^2 g^{-1} olivine), M_{olivine} is the molar mass of olivine (g^{-1} mol) and Ω is the saturation state. Saturation occurs when dissolution products build up in the pore water, eventually reaching thermodynamic equilibrium (

290 $\Omega = 1$ meaning full saturation) and thus impeding further dissolution (Köhler et al., 2010). Montserrat et al. (2017) and Flipkens et al. (2023b) reported that saturation effects slowed down dissolution rates in some of their long-term laboratory experiments. Yet, little is known about how the saturation state impacts olivine weathering in the pore water of marine sediments. The three CESW application scenarios considered (Fig. 2b–d) all assume some form of continuous exchange of the (pore) water surrounding the olivine, thereby preventing saturation effects. However, saturation effects may occur in cohesive

295 sediments with little physical or biological irrigation. Potential saturation effects on olivine dissolution in marine sediments hence comprise an important aspect of investigation in future studies. In the following sections, we discuss the factors affecting k_{d} and A_{surf}, and their effects on the olivine dissolution rate.

3.1.1 The intrinsic dissolution rate of olivine

Many studies have investigated the k_{d} value of forsterite in aqueous solutions with a high fluid-to-mineral ratio, thus enabling

300 experimental conditions to remain far from thermodynamic equilibrium (Bailey, 1976; Blum and Lasaga, 1988; Chen and Brantley, 2000; Eriksson, 1982; Giammar et al., 2005; Golubev et al., 2005; Grandstaff, 1986; Hänchen et al., 2006, 2007; Hausrath and Brantley, 2010; Luce et al., 1972; Oelkers, 2001a; Olsen et al., 2015; Olsen and Donald Rimstidt, 2008; Pokrovsky and Schott, 2000; Prigiobbe et al., 2009; Rosso and Rimstidt, 2000; Shirokova et al., 2012; Siegel and Pfannkuch, 1984; Van Herk et al., 1989; Wogelius and Walther, 1991). The resulting data have been synthesized in several reviews

305 (Heřmanská et al., 2022; Oelkers et al., 2018; Rimstidt et al., 2012). This interest in olivine dissolution kinetics is due to its relatively simple reaction mechanism, its potential role in CO_2 sequestration (Heřmanská et al., 2022; Oelkers et al., 2018; Rimstidt et al., 2012), and more recently in reconstructing the past climate on Mars (Gaudin et al., 2018; Hausrath and Brantley, 2010; Niles et al., 2017; Olsen et al., 2015). These studies show that k_{d} primarily is affected by pH and temperature (Brantley et al., 2008; Crundwell, 2014; Heřmanská et al., 2022; Olsen, 2007; Pokrovsky and Schott, 2000; Rimstidt et al., 2012;

310 Wogelius and Walther, 1991). The following empirical equations for the dissolution rate constant, valid between $0 < \mathrm{pH} < 14$ and $0°C < T < 150°C$, have been provided (Heřmanská et al., 2022; Rimstidt et al., 2012):

$$\log(k_{\mathrm{d}}) = 5.17(0.16) - 0.44(0.01)pH - 3675(47.0)1/T \qquad (\mathrm{pH} < 5.6) \qquad (6)$$

$$\log\left(k_\mathrm{d}\right) = 2.34(0.40) - 0.22(0.02)\,pH - 3179(143)1/T \qquad (\mathrm{pH} > 5.6) \tag{7}$$

It is important to note that k_d values are normalized to the specific surface area of the olivine grain (section 3.1.5), which is
315 represented in two ways: either the actual surface area as estimated via Brunauer, Edward, and Teller (BET) analysis (A_BET)
or the geometrical surface area (A_geo), which assumes that the dissolving grain is a perfect sphere. The choice of surface
normalization procedure critically influences the resulting k_d values, as A_BET can be considerably larger than A_geo. The
Rimstidt relations Eq. (6) and Eq. (7) are normalized using A_BET, so the resulting k_d values should not be compared with those
normalized using A_geo without proper conversion.

320 Here, we discuss the impact of pH and temperature on k_d (Fig. 4), as well as the effect of salinity, due to its relevance for
coastal environments. Some studies have also suggested that the CO_2 concentration can affect the dissolution rate of olivine at
a pH higher than 6 (Pokrovsky and Schott, 2000; Wogelius and Walther, 1991). However, more recent studies found no explicit
CO_2 effect when correcting for the change in pH caused by elevated CO_2 concentrations (Golubev et al., 2005; Prigiobbe et
al., 2009). As such, CO_2 appears to affect olivine dissolution only indirectly through a change in pH. Rates of k_d in Fig. 4
325 were compiled from Rimstidt et al. (2012) and Heřmanská et al. (2022), supplemented with additional data (Flipkens et al.,
2023b; Gerrits et al., 2020; Hausrath and Brantley, 2010; Lunstrum et al., 2023; Montserrat et al., 2017; supplementary file
1.1).
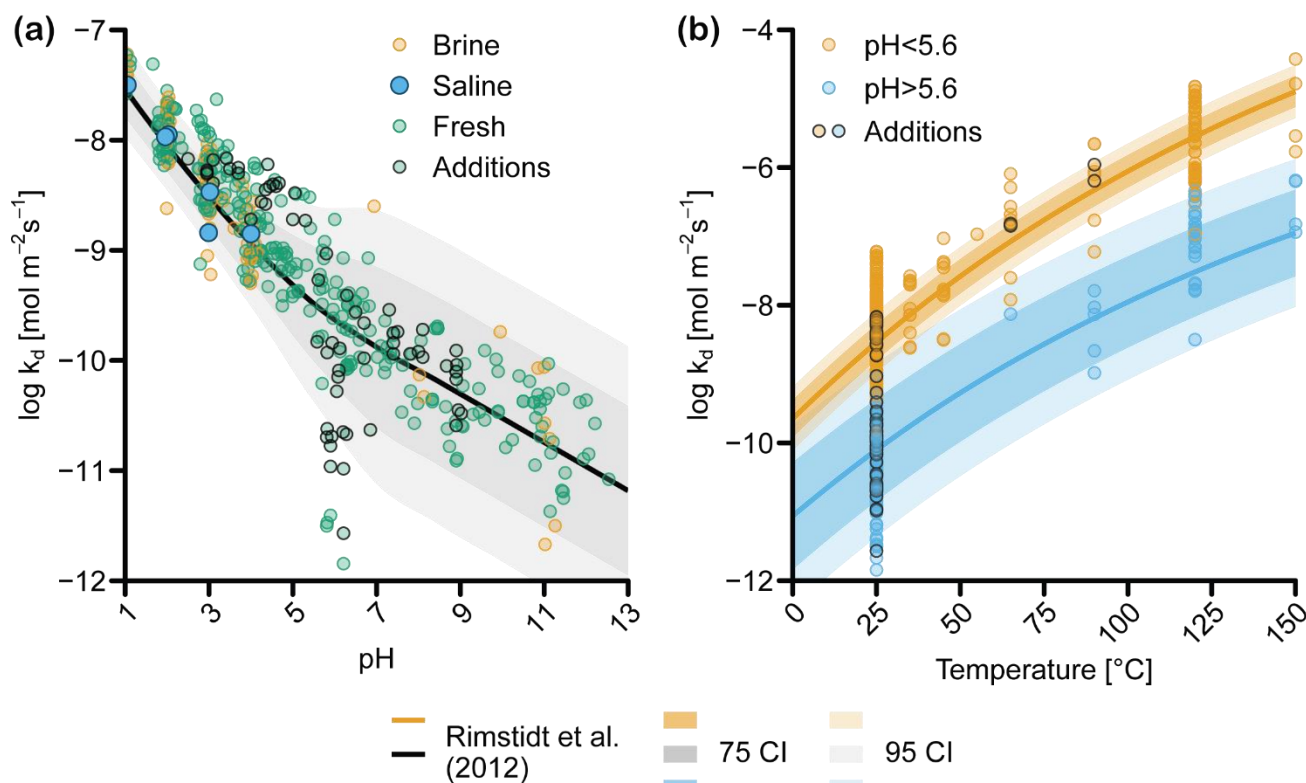
330

Figure 4. (a) Forsterite dissolution rates (k_d), adjusted to 25°C, as a function of pH according to the rate equations from Rimstidt et al. (2012). Data are normalized to BET surface areas and categorized according to salinity (freshwater < 0.6 mol l^{-1}, saline = 0.6–0.85 mol l^{-1}, brine > 0.85 mol l^{-1}). The uncertainty band was derived using the standard error for each parameter (supplementary file 1.2). (b) k_d as a function of temperature. The Rimstidt et al. (2012) rate equation was solved for pH 3.13 and 8.22, respectively, which were the average pH values of experiments at acidic (pH < 5.6) and basic (pH > 5.6) conditions. "Additions" marks data from dissolution experiments where factors other than pH and temperature were investigated (e.g., the addition of dissolved organic matter, the addition of aluminum), which may have affected k_d (supplementary file 1.1).

3.1.2 Impact of pH on olivine dissolution

The olivine dissolution rate constant k_d follows a log-linear dependency on pH (Fig. 4a). Different mechanisms have been suggested to explain the observed change in dissolution rate between acidic and basic conditions. Pokrovsky and Schott (2000) argued that different reaction mechanisms occur at pH < 9 and pH > 9. For acidic and slightly alkaline conditions (pH < 9), Mg^{2+}/Fe^{2+} ions within the olivine are exchanged with two protons, creating a silica-rich, Mg/Fe-free protonated surface precursor complex followed by the sorption of one proton on two polymerized silica tetrahedra (Pokrovsky and Schott, 2000). A lower pH increases the concentration of free protons in solution, which can exchange with Mg/Fe in the olivine and accelerate the release of silica tetrahedra and hence the dissolution of olivine (Oelkers et al., 2018; Pokrovsky and Schott, 2000). In basic conditions (pH > 9), silica would be preferentially released, and Mg/Fe sites hydrated, forming (Mg/Fe)OH$_2^+$ species that control the dissolution (Pokrovsky and Schott, 2000).

Rimstidt et al. (2012) also proposed two separate pH regimes, but with a transition at pH 5.6 rather than pH 9 (Fig. 4a). The dependency of k_d on pH is twice as strong at pH < 5.6 compared to pH > 5.6. While Rimstidt et al. (2012) point out that the apparent break in the data could be due to the relative paucity of rate measurements for pH > 6 and temperatures below 25°C,

350 they also suggest that different mechanisms may drive the dissolution at low and high pH, leading to the two rate reactions presented in Eq. (6) and Eq. (7) (Rimstidt et al., 2012). Based on the dataset from Rimstidt et al. (2012), Crundwell (2014) proposed that an additional step occurs in basic and slightly acidic conditions (pH > 5.6), whereby H^+ ions absorb at the inner Helmholtz layer of the silicate mineral. This absorption would enable the release of Mg/Fe to the solution, after which the adsorbed H^+ ion can react with the silica tetrahedra to form H_4SiO_4, which goes into solution. This reaction mechanism explains

355 the slope change at a pH~5.6 (Fig. 4a). In conclusion, there seems to be experimental and theoretical support for two dissolution mechanisms of olivine depending on pH regime, with considerably higher dissolution rates at lower pH (< 5.6).

The range of pH conditions relevant to CESW under field conditions is relatively narrow compared to the range shown in Fig. 4a. While the pH of coastal seawater is relatively high and shows minor variation (pH ≈ 7.9–8.3), the pH in coastal sediments is generally more acidic and also variable with depth (pH ≈ 6–8) (Cai et al., 1995; Pfeifer et al., 2002; Rao et al., 2012; Silburn

360 et al., 2017; Widdicombe et al., 2011; Zhu et al., 2006). Olivine is therefore expected to show higher dissolution rates in the sediment compared to the water column (Meysman and Montserrat 2017). However, accurate descriptions of the spatial and temporal variability of the pore-water pH are currently lacking (Silburn et al., 2017). The pore-water pH is determined by microbial redox reactions, as well as mineral dissolution and precipitation, which in turn are controlled by sediment characteristics and the presence of burrowing fauna. Within the same sediment, spatial and temporal pH variations are the

365 result of seasonal changes in the organic matter supply, which affects the sedimentary O_2 demand (Silburn et al., 2017; Widdicombe et al., 2011), alters the physical advection and biological irrigation (Meysman et al., 2007), and changes the microbial activity (Meysman et al., 2015). In addition to being a master variable for olivine dissolution, pH also determines the possibility of secondary reactions (e.g. sepiolite formation). The lack of data on olivine dissolution rates at pore-water pH and the absence of suitable spatial maps of sediment pH within coastal environments emerge as important research gaps that

370 hamper the prediction of CO_2 sequestration by CESW. Careful monitoring of sediment pH during future field applications is required to designate the best application areas for CESW.

3.1.3 Impact of temperature on olivine dissolution

The k_d value increases with temperature, and this relationship is classically described via the Arrhenius equation (Casey and Sposito, 1992; Oelkers et al., 2018):

375
$$k_d = A_0 \exp\left(\frac{-E_a}{RT}\right) \tag{8}$$

where A_0 refers to the temperature-independent pre-exponential factor (mol m^{-2} s^{-1}), E_a stands for the apparent activation energy of olivine dissolution (J mol^{-1}), R is the gas constant (J K^{-1} mol^{-1}), and T is the temperature (K). The Arrhenius equation can be used to rescale k_d values to different temperatures via the relation (Montserrat et al., 2017):

$$k_{d2} = k_{d1} \cdot \exp\left(\frac{E_a}{R}\left(\frac{1}{T_2} - \frac{1}{T_1}\right)\right) \tag{9}$$

380 Past olivine dissolution studies have typically been conducted at temperatures of 25–125°C (Fig. 4b), from which E_a values of 70.4 kJ mol^{-1} for pH < 5.6 and 60.9 kJ mol^{-1} for pH > 5.6 have been derived (Rimstidt et al., 2012). However, there is a clear lack of rate studies within the environmentally relevant temperature range of 0–25°C, which reflects the natural variation of annual mean temperatures within the seafloor. The few experiments investigating dissolution below 25°C have found markedly lower E$_a$ values of 31–33 kJ mol^{-1} (Hausrath and Brantley, 2010; Niles et al., 2017), but these low-temperature activation

385 energies were derived from experiments conducted in highly acidic conditions (pH < 2; Hausrath and Brantley 2010; Niles et al. 2017). Still, they suggest that the activation energy of 70.4 kJ mol^{-1} at pH < 5.6 used by (Rimstidt et al., 2012) may not hold for the temperature range 0–25°C. No studies have been conducted at environmentally relevant conditions (pH ~ 8 and temperature 0–25 °C), so E_a appears to be uncertain for this range, pinpointing an area for further research. By applying the Arrhenius equation and using an apparent activation energy of 60.9 kJ mol^{-1} (Rimstidt et al., 2012), we find that olivine

390 dissolves about 10 times faster at 25°C compared to at 0°C (Hangx and Spiers, 2009). From a CESW perspective, the geographical location is thus expected to impact the olivine dissolution rate profoundly. Spreading olivine in a polar region (temperature range 0–10°C) compared to application in tropical regions (temperature range 20–35°C) would decrease the dissolution rate by a factor of 2.4–21.0. The sensitivity of k_d to temperature further implies that dissolution rates may vary with the seasons in temperate environments. This potentially temporal variability in the olivine dissolution rate complicates

395 the MRV of CESW, as multiple measurements of olivine dissolution rates would be required at suitable temporal resolution throughout the seasonal cycle, thus increasing the costs of monitoring schemes.

3.1.4 Impact of salinity on olivine dissolution

The dissolution rate constant k_d decreases at high salinities (brine, ionic strength > 6 mol kg solution^{-1}), as the activity coefficient of water (a_{H_2O}) is lowered when the ionic strength of an aqueous solution increases (Olsen et al., 2015; Prigiobbe

400 et al., 2009). As a_{H_2O} expresses how easily the water can interact with the olivine, a high ionic strength of the solution indirectly affects the dissolution rate by lowering the "effective concentration" of the water needed to react with olivine. When correcting for the change in a_{H_2O}, salinity does not noticeably affect the dissolution rate of olivine below an ionic strength of 12 mol kg^{-1} (for reference: open ocean seawater has an ionic strength of ~0.7 mol kg^{-1}; Olsen et al. 2015). It should be noted, however, that most olivine dissolution experiments have been conducted in deionized water. Furthermore, olivine dissolution

405 experiments at seawater salinities have mostly been conducted within the low pH range 1–4 (Fig. 4a). Accordingly, the effect

of salinity on olivine dissolution at environmental field conditions (ionic strength 0–0.7 mol kg^{-1}, pH 6–8.3) has not been explicitly assessed, but salinity variations are unlikely to have a major effect.

3.1.5 Specific surface area

The specific surface area of the olivine grains is a crucial parameter since it is used to normalize k_d under the assumption that
410 dissolution rates are surface-controlled (Brantley et al., 2008). Typically, surface areas are reported as either geometric (A_{geo}) or BET (A_{BET}) surface areas (Brantley et al., 2008; Brunauer et al., 1938; Rimstidt et al., 2012). When using A_{geo}, one assumes that the mineral grain adopts a spherical shape (Brantley et al., 2008). Accounting for spherical geometry, the geometric specific surface area is calculated for a grain size distribution consisting of *n* classes via (Flipkens et al., 2023b; Rimstidt et al., 2012):

415
$$A_{geo} = \sum_{i=1}^{n} \left(\varphi_i \frac{6V_{olivine}}{M_{olivine}D_{e_i}} \right) \tag{10}$$

Here, φ_i is the forsterite fraction of a certain grain diameter class *i*, $V_{olivine}$ is the molar volume of forsterite (4.365×10^{-5} m^3 mol^{-1}), $M_{olivine}$ is the molar mass of forsterite (140.69 g mol^{-1}), and D_e is the equivalent diameter (m) of a grain size interval (Tester et al., 1994):

$$D_e = \frac{D_{max} - D_{min}}{\ln\left(D_{max}/D_{min}\right)} \tag{11}$$

420 In Eq. (11), the grain-size distribution is assumed to be constant over the given range. At small particle size intervals, the arithmetic mean of the maximum (D_{max}) and minimum (D_{min}) grain diameter of a particular grain size class will be close to D_e. For large intervals, D_e is smaller than the arithmetic mean since smaller particles contribute more to the area than large particles (Rimstidt et al., 2012; Tester et al., 1994).

The BET-based quantity A_{BET} is obtained by measuring the adsorption of a monolayer of inert gas (Kr, N$_2$) on a sample of
425 grains (Brantley et al., 2008; Brantley and Mellott, 2000). Since the size of a water molecule is similar to that of N$_2$ and Kr, the BET method is considered to be a good proxy for characterizing the interaction between the mineral surface and water (Rimstidt et al., 2012). BET measurements are typically reported for the fresh olivine grains introduced at the start of the experiment, and because of the limited duration of experiments, it is assumed that the specific surface area does not markedly change (e.g. Hänchen et al. 2006; Pokrovsky and Schott 2000; Oelkers 2001b). However, under field conditions, the full
430 dissolution of olivine sand may require 10-500 years, depending on the initial grain size. Accordingly, the evolution of A_{BET} as the grain dissolves is unknown, which must be considered in future long-term experiments.

The relation between A_{geo} and A_{BET} is given by the grain roughness (R_S), which is defined as (Brantley et al., 2008; Brantley and Mellott, 2000; Oelkers et al., 2018):

$$R_S = \frac{A_{BET}}{A_{geo}} \tag{12}$$

435 Fig. 5a shows the data distribution of R_S values as reported in literature, which is largely based on Rimstidt et al. (2012) with a few additions. Following Rimstidt et al. (2012), we excluded data where R_S was larger than 10, as these values likely result from reading or calibration errors and retention of fine particles on the grain surfaces. Additionally, in our data compilation, we omitted the data from Olsen et al. (2015), as they derived a BET value using an empirical rate equation from A_{geo} rather than a direct measurement. The R_S value in our compiled dataset ranges between 2 and 8, with a mean of 5.2 (Fig. 5a).

440 Accordingly, there is considerable variation in grain roughness R_S between the olivine sand used in experiments. Moreover, there is no strong correlation between A_{BET} and A_{geo} (Fig. 5b). Overall, R_S tends to increase at smaller grain sizes (Strefler et al., 2018), albeit with substantial variability. Overall, the source of this variability remains poorly understood, but it has been shown that the type of mill used to grind olivine source can significantly alter grain roughness R_S, providing highly different A_{BET} values for the same A_{geo} (Summers et al., 2005). The lack of a clear empirical relation between A_{BET} and A_{geo}

445 complicates model-based predictions of the dissolution rate in future CESW applications. Therefore, an accurate characterization of R_S is highly advisable in future CESW experiments and applications. This issue also highlights the importance of a consistent normalization of reported dissolution rate constants k_d. Rimstidt et al. (2012) argued that geometric-based normalization of dissolution rates can be useful for practical reasons, as it reduces analysis costs and avoids errors during BET measurements. However, using the actual A_{BET} value is advantageous due to the poor predictability of R_S.

450
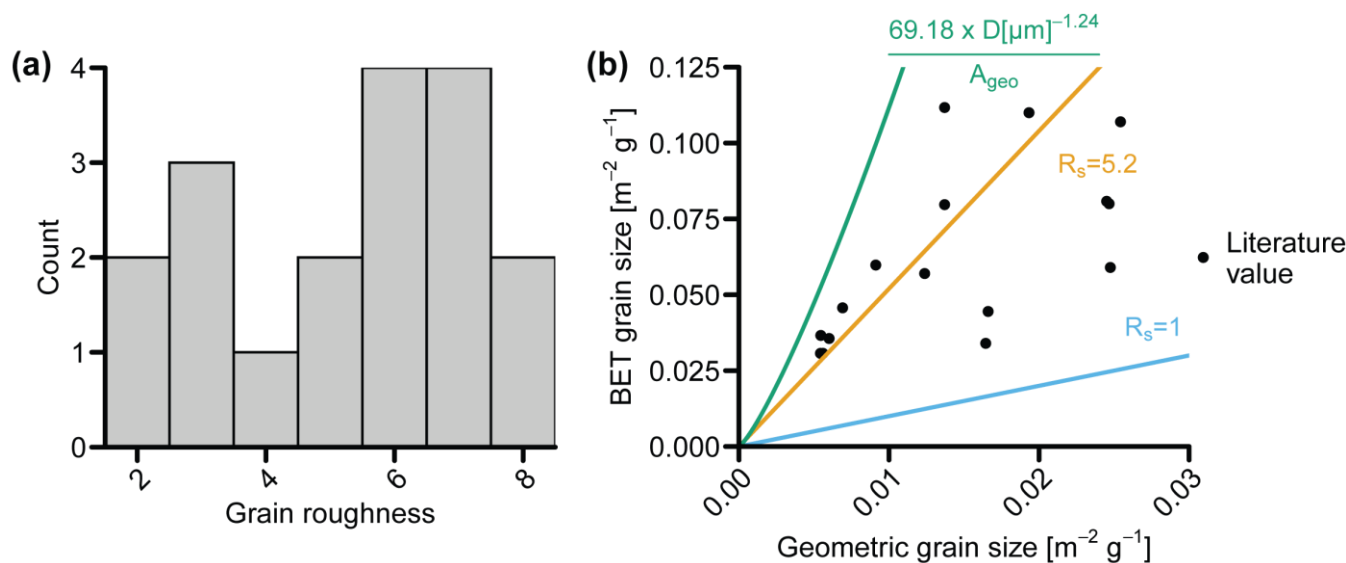
Figure 5. (a) Histogram of grain roughness (R_S) values in the compiled literature (supplementary file 2). (b) Relationship between the geometric surface area (A_{geo}) and BET surface area (A_{BET}). The empirical equation from Strefler et al. (2018) (in green) corresponds to an average $R_S \sim 12$. $R_S = 5.2$ is the mean grain roughness in the compiled literature, $R_S = 1$ shows the relationship for a perfect sphere.

455 Furthermore, it should be noted that the link between specific surface area and mineral reactivity can change with time. In the olivine dissolution experiments conducted by Grandstaff (1978), A_{BET} increased substantially over five days (pH = 2.6) as

etch pits and cracks formed. These dissolution features have also been found in naturally weathered olivine (Velbel, 2009) as well as laboratory olivine dissolution experiments (e.g. Flipkens et al. 2023b), and hence, the assumption that A_{BET} remains constant in time throughout long-term CESW applications is likely not valid. Interestingly, this large increase in A_{BET} was

460 not accompanied by a concurrent increase in dissolution rate (Grandstaff, 1978), highlighting that there can be an increase in the total surface area while the reactive surface area stays the same. Unfortunately, temporal variation in reactive surface area is not easily monitored (Brantley et al., 2008; Oelkers et al., 2018; Rimstidt et al., 2012). Potentially, insight into the evolution of the reactive surface area over the whole weathering trajectory might be attained by looking at natural deposits of olivine sand with different ages (e.g. the older olivine deposit at Papakōlea beach in Hawaii versus the much younger Tremblet Beach

465 in La Reunion). Comparing A_{BET} and k_{d} values of freshly mined olivine with those of naturally occurring olivine sand could indicate how olivine weathering rates in CESW applications may be affected over longer time scales.

3.1.6 Passivating layers

Passivating layers are any coatings on the olivine surface, biogenic or inorganic, that slow down dissolution. Microbial biofilms growing on olivine grains have been found to weakly inhibit dissolution (Shirokova et al., 2012), and precipitation of secondary

470 minerals (sections 3.3.1–3.3.2) may also create passivating layers (Béarat et al. 2006; Sissmann et al. 2013). The occurrence of amorphic passivating layers on olivine grains and their effect on dissolution has been discussed in detail elsewhere (Pokrovsky and Schott, 2000; Béarat et al., 2006; Daval et al., 2011; Sissmann et al., 2013; Johnson et al., 2014), and was also extensively covered in the recent review by Oelkers et al. (2018). Amorphic layers may form as Mg^{2+} is leached from the olivine surface, causing the remaining silica-rich layer to repolymerize and form an amorphous SiO_2 coating (Béarat et al.,

475 2006; Oelkers et al., 2018). However, SiO_2 coatings are only inhibiting when Fe^{3+} (derived from the fayalite component of the olivine itself) is incorporated into their structure (Oelkers et al., 2018). Recent experiments indicate that microbial and fungal uptake of Fe can prevent the build-up of these passivating layers and increase olivine weathering rates (Gerrits et al., 2020, 2021; Lunstrum et al., 2023; Torres et al., 2019). However, when no Fe uptake occurs, the effect of microbial biofilms on dissolution is less conclusive and appears to be slightly inhibiting (Shirokova et al., 2012). Future studies should consider *in*

480 *situ* microbial effects on olivine dissolution, which is likely relevant for weathering in natural systems.

In their olivine dissolution experiments in seawater, Montserrat et al. (2017) observed a decreased Mg-to-Si atomic ratio on the surface of reacted forsterite compared to the initial substrate, indicating that a Mg-leached layer had formed as was proposed by Hellmann et al. (2012) and Maher et al. (2016). In contrast, Fuhr et al. (2022) found no such Mg-depletion, postulating that the high Mg concentrations in their artificial seawater prevented depletion at the olivine surface. Flipkens et

485 al. (2023) mimicked the wave action in the coastal zone by continuously rotating olivine sand to induce grain collision, hypothesizing that grain abrasion could decrease the formation of passivating layers. These experiments revealed that physical agitation increases the olivine dissolution rate by a factor of 8–19 compared to stagnant conditions. However, Flipkens et al. (2023) only found slight variations in the Mg-to-Si atomic ratio on the olivine grain surface between treatments (with large variations on the same grain), indicating that the formation of Mg-depleted layers was minimal in both the stagnant and high

490   rotation treatments. Flipkens et al. (2023) hence attributed most of the dissolution rate enhancement to water flushing rather
than physical abrasion of the grain surface.

Until now, there is little knowledge on passive layer formation on olivine grains under *in situ* marine conditions relevant to
CESW. Previous experiments reporting on passivating layer formation have been typically conducted in freshwater at elevated
CO_2 pressure (135–250 bar) and temperature (60–185°C) (Béarat et al., 2006; Daval et al., 2011; Johnson et al., 2014; Maher

495   et al., 2016; Sissmann et al., 2013). Consequently, the possibility of passive layer formation in coastal sediment conditions
warrants further research. Several processes may potentially counteract such layer formation during CESW application. In the
bedload scenario, olivine particles will be subjected to the action of waves and currents, possibly removing passivating layers
(Flipkens et al., 2023b). Moreover, when olivine is applied in cohesive sediment, the particles may be ingested by infauna,
which could prevent passivating layer formation (Meysman and Montserrat, 2017). Although initial studies suggest that

500   substantial formation of passivating layers seems unlikely (Bach, 2024; Flipkens et al., 2023b; Meysman and Montserrat, 2017;
Montserrat et al., 2017), the formation of a thin cation-depleted layer cannot be completely ruled out. Future work should
investigate the precise conditions under which these layers form and how they impact weathering rates (Montserrat et al., 2017;
Oelkers et al., 2018; Palandri and Kharaka, 2004; Pokrovsky and Schott, 2000), as well as further quantify the effect of grain
abrasion on passivating layer formation (Flipkens et al., 2023b). Likewise, the prevalence and effect of biofilm formation on

505   olivine dissolution rates need to be addressed in future CESW studies.

3.2 The stoichiometric alkalinity production factor

Chemical weathering of olivine is commonly described as a reaction where pure forsterite completely dissociates into its
constituent ions Mg^{2+} and SiO_4^{4-}, thus generating 4 moles of alkalinity per mole of olivine dissolved (γ_{A_T} = 4; Table 3)
(Meysman and Montserrat, 2017; Oelkers et al., 2018; Schuiling and Krijgsman, 2006). However, olivine dissolution may also

510   be incomplete and deviate from this idealized primary weathering reaction. During incomplete dissolution, alteration products
such as serpentine and sepiolite can be formed, and the alkalinity production is lowered (Table 3). Thermodynamic modeling
shows that sepiolite formation and serpentinization are theoretically possible when olivine is exposed to seawater (Griffioen,
2017). Clay formation has been proposed as a third potential mechanism of incomplete dissolution (Deer et al., 2013; Delvigne
et al., 1979). It should be noted that both sepiolite and serpentine are Mg-silicates and hence can further dissolve and release

515   additional alkalinity when exposed to the right conditions. Both sepiolite and serpentine have been considered as source
minerals for use in CDR (e.g. Alexander et al. 2007; Dichicco et al. 2015; Farhang et al. 2017; Mulders et al. 2018); however,
the dissolution rates of these minerals are orders of magnitudes lower than that of olivine (Table 2). Therefore, we consider
sepiolite and serpentine unreactive on the required timescale for CDR (< 100 years) and so we will not further discuss their
CO_2 sequestration potential.

520   To quantify γ_{A_T} , one must assess whether olivine dissolution will run to completion during CESW application under natural
conditions. Recently, several experiments have been conducted on the dissolution of olivine in both artificial seawater (e.g.
Montserrat et al. 2017; Rigopoulos et al. 2018; Fuhr et al. 2022) and natural seawater (Flipkens et al., 2023b; Montserrat et al.,

2017). These studies provide a first insight into the specific alteration products that can form during enhanced olivine weathering (as detailed below). However, it is unclear to what extent the reaction conditions (e.g. pH and chemical

525 environment) utilized in these laboratory experiments are relevant for olivine dissolution in sediments, and studies conducted on olivine weathering in sediment have so far not addressed this issue (Bach, 2024; Fuhr et al., 2023).

Table 3. Dissolution reactions suggested to occur during CESW with forsterite. [a]No alkalinity is produced, but the serpentinization reaction leads to the formation of magnesium carbonate, sequestering 0.5 mol DIC per mol forsterite. [b]The reaction is unbalanced
530 **since iddingsite never consists of a single phase and the composition is very variable.**

Reaction	Mechanism	γ_{A_T}
Primary weathering reaction[1]	$Mg_2SiO_4 + 4H_2O \rightarrow 4OH^- + 2Mg^{2+} + H_4SiO_4$	4
Sepiolite formation[2]	$\frac{3}{2}Mg_2SiO_4 + \frac{15}{4}H_2O \rightarrow 4OH^- + \frac{1}{4}Mg_4Si_6O_{15}(OH)_2 \cdot 6H_2O + 2Mg_2^+$	2.67
Serpentinization[3]	$Mg_2SiO_4 + \frac{4}{3}H_2O + \frac{1}{3}SiO_2 \rightarrow 0OH^- + \frac{2}{3}Mg_3Si_2O_5(OH)_4$	0
	$MgSiO_4 + \frac{3}{2}H_2O \rightarrow \frac{1}{2}Mg_3Si_2O_5(OH)_4 + \frac{1}{2}Mg(OH)_2$	0
	$MgSiO_4 + H_2O + \frac{1}{2}CO_2 \rightarrow \frac{1}{2}Mg_3Si_2O_5(OH)_4 + \frac{1}{2}MgCO_3$	0a
Iddingsitization[4,5,b]	$(Mg,Fe)_2SiO_4 \rightarrow 0OH^- + MgO \cdot Fe_2O_3 \cdot 3SiO_2 \cdot 4H_2O$	0

[1](Meysman and Montserrat, 2017), [2](Griffioen, 2017), [3](Deer et al., 2013), [4](Edwards, 1938), [5](Wilson, 2004)

3.2.1 Sepiolite formation

Sepiolite ($Mg_4Si_6O_{15}(OH)_2 \cdot 6H_2O$) is a clay mineral that belongs to the group of phyllosilicates and is the only Mg-silicate that can precipitate from oxic seawater in the absence of aluminum (Griffioen, 2017). Alkalinity is still generated when sepiolite

535 precipitates during olivine weathering $(\gamma_{ALK} = 2.67)$ but to a lesser extent than the complete dissolution reaction (Table 3). Sepiolite formation has been observed in low-temperature systems, such as near hydrothermal vents, in marine and lacustrine sediments, and in volcanic deposits (Mulders and Oelkers, 2020; Wollast et al., 1968). While the exact mechanism of sepiolite formation is the subject of ongoing debate, it is generally thought that sepiolite only forms in seawater conditions under specific circumstances. Sepiolite formation requires a high pH > 8 (Baldermann et al., 2018; Wollast et al., 1968) and elevated

540 concentrations of dissolved Si and Mg^{2+}, caused, for example, by evaporation (Baldermann et al., 2018; Tosca and Masterson, 2014). Since seawater contains high concentrations of Mg^{2+} (0.05 mol kg^{-1}; (Johnson et al., 1992)), dissolved Si is generally the limiting element for sepiolite formation in seawater (Baldermann et al., 2018). However, even at a steady supply of dissolved Si (e.g., through silicate weathering or dissolution of biogenic opal) and at a high pH, precipitation of sepiolite remains slow (~10^{-12} mol s^{-1}) at ambient coastal seawater temperatures (Baldermann et al., 2018). In marine conditions,

545 sepiolite formation is further impeded by the presence of sodium ions (Na^+), which affects the speciation of dissolved silicate,

and by the presence of sulfate ions (SO_4^{2-}), which lowers the availability of free Mg^{2+} through the formation of $MgSO_4$ complexes (Baldermann et al., 2018; Tosca and Masterson, 2014). Other cations (e.g., Ca^{2+}, K^+) can also absorb onto the sepiolite surface, preventing further growth (Baldermann et al., 2018).

While model calculations have shown sepiolite oversaturation in experimental studies on olivine dissolution in seawater
550 (Flipkens et al., 2023b; Fuhr et al., 2022; Rigopoulos et al., 2018), the experimental documentation of sepiolite formation remains inconclusive. Effectively, sepiolite has only been directly observed once (Rigopoulos et al., 2018), while another study found a mix of silicate-bearing phases on weathered olivine grains, potentially including sepiolite (Fuhr et al., 2022). In contrast, Montserrat et al. (2017) and Flipkens et al. (2023) found no phyllosilicate precipitates on weathered olivine grains. Oelkers et al. (2018) suggested that sepiolite formation in the experiments by Rigopoulos et al. (2018) could have been
555 provoked by the buildup of Mg^{2+} in the supernatant solution. However, this is unlikely due to the high background concentration of Mg^{2+} in seawater. Instead, a rapid pH increase (from 8 to >8.6) caused by rock flour addition may have caused the observed sepiolite precipitation, since a pH increase from 8 to 9 can increase the sepiolite growth rates by an order of magnitude (Baldermann et al., 2018). Overall, due to the generally low pH of pore water and low ambient temperatures in coastal environments, sepiolite formation is unlikely during CESW application, but more targeted studies are needed to confirm
560 this.

3.2.2 Serpentinization

During serpentinization, forsterite is transformed into serpentine, sometimes in parallel with the formation of brucite ($Mg(OH)_2$) or magnesite ($MgCO_3$) (Table 3) (Deer et al., 2013; Griffioen, 2017). No alkalinity is formed during serpentinization $\left(\gamma_{A_T} = 0 \right)$, but precipitation of magnesite leads to direct sequestration of CO_2 in the mineral. In marine
565 environments, serpentine is typically formed over a wide temperature range (50–600°C) in high-temperature hydrothermal systems, subduction zones, and mid-ocean ridges (Alt et al., 2012, 2013; Schwarzenbach et al., 2012). Serpentinization has also been found to occur at lower temperatures (from 200°C down to ~10°C) in hydrothermal deposits with high sulfide content, such as the Lost City hydrothermal field (Mid-Atlantic ridge) (Alt et al., 2012; Mével, 2003; Neubeck et al., 2011). However, serpentinization is unlikely during CESW as it typically occurs at temperatures much higher than in coastal systems
570 (0–35°C). Serpentinization with magnesite production is particularly unlikely as this mineral typically does not form under ambient marine conditions (section 3.3.1), and brucite formation is unfavorable at pH values below 8 (Griffioen, 2017; Wollast et al., 1968).

Up until now, serpentine has not been found to form in olivine dissolution experiments using oxic seawater (Flipkens et al., 2023b; Fuhr et al., 2022; Montserrat et al., 2017; Rigopoulos et al., 2018), although both Fuhr et al. (2022) and Flipkens et al.
575 (2023) calculated that serpentine was oversaturated throughout most of their experiments. Fuhr et al. (2022) and Flipkens et al. (2023) also advanced that talc ($Mg_3Si_4O_{10}(OH)_2$) formation is possible. However, talc formation from olivine proceeds via serpentinite, and these reactions require high pressure and temperature (200–650°C; Bucher and Grapes 2011; Deer et al. 2013). As such, the formation of talc is unlikely in coastal settings.

3.2.3 Formation of other clay minerals

580 Olivine can transform into complex assemblages of clay minerals and iron hydroxides, often identified as bowlingite (old name for saponite) and iddingsite. The relative abundance of bowlingite and iddingsite is dependent on the oxidation state of Fe, with bowlingite being formed under non-oxidative conditions and iddingsite under oxidative conditions (Deer et al., 2013; Smith et al., 1987). Delvigne et al. (1979) and Wilson (2004) state that the saturation state of the system is critical for clay mineral formation. When rock-to-fluid ratios are low, Mg^{2+} and Fe^{2+} from olivine dissolution escapes into solution, where Fe^{2+}

585 precipitates as iron (oxyhydr)oxides in oxic conditions. When rock-to-fluid ratios are high, dissolution products are concentrated, and smectite (clay mineral group including bowlingite) formation is promoted (Delvigne et al., 1979; Gaudin et al., 2018). Even though clay formation from natural olivine dissolution has been historically well-documented for soils (Baker and Haggerty, 1967; Brown and Stephen, 1959; Edwards, 1938; Eggleton, 1984; Sherman and Uehara, 1956; Smith et al., 1987; Sun, 1957; Wilshire, 1958), this process has not been investigated in seawater conditions. As such, we lack information

590 about clay formation during CESW.

3.2.4 Implications for CESW

Experiments on olivine dissolution in seawater have so far provided little evidence for incomplete dissolution of olivine. In one instance, small amounts of sepiolite formation were reported (Rigopoulos et al., 2018), whereas no serpentinization has been observed (Montserrat et al., 2017; Rigopoulos et al., 2018; Fuhr et al., 2022; Flipkens et al., 2023b). The formation of

595 clay minerals has not been specifically investigated. It is important to note that all experiments have been conducted in oxygenated seawater and hence are not completely representative of sedimentary conditions (e.g. in terms of O_2 and pH). Compared to seawater, the typical pH of pore waters is lower (pH 6–8), which decreases the likelihood of sepiolite formation (Wollast et al., 1968; Baldermann et al., 2018). Most olivine dissolution experiments have also been conducted in closed systems, where reaction products are allowed to build up (e.g. Montserrat et al., 2017; Rigopoulos et al., 2018; Fuhr et al.,

600 2022). Under CESW application, the weathering will take place in an open environment. Reaction products from olivine weathering will be released into the pore water, which is then flushed either through physical advection (wave or current action) or through bioirrigation (Meysman and Montserrat, 2017). It should be noted that Bach (2024) and Fuhr et al. (2023) included sediment in their CESW experiments; however, they did not specifically investigate the formation of sepiolite, serpentine, or clays. In conclusion, the physiochemical conditions in coastal sediments seem unfavorable for forming sepiolite

605 and serpentine. In contrast, the formation of clay minerals could be relevant depending on flushing conditions, and their formation during CESW warrants further research.

3.3 Secondary reactions

The dissolution of olivine in the sediment releases alkalinity to the pore water. To enable CO_2 sequestration, this alkalinity must be transferred across the sediment-water interface to the overlying water column (Fig. 2). However, the build-up of

dissolution products in the sediment can promote the precipitation of "secondary" minerals, which can consume the alkalinity generated from olivine weathering. The secondary reactions most likely to occur in aquatic sediment environments are carbonate and iron mineral precipitation (Table 4) (Griffioen, 2017). In general, the occurrence of secondary reactions is regulated by the saturation state of a particular mineral, the governing kinetics, and the availability of nucleation sites (Morse et al., 2007). As such, olivine weathering has recently been suggested to inhibit the metabolic dissolution of carbonates naturally present in the sediment (Bach, 2024). As such, olivine dissolution decreases the natural alkalinity generation in the sediment, compromising the "additionality principle": the alkalinity generated by olivine dissolution no longer fully adds to the natural alkalinity generation. Secondary reactions and the inhibition of natural alkalinity generation thus decrease the alkalinity efflux to the overlying water, as described by the parameter $0 \leq \mu_{SR} \leq 1$.

Table 4. Secondary precipitation reactions that can occur during CESW. [a]When calcium carbonate (CaCO₃) is formed, 1 mol DIC is effectively sequestered within the mineral. Therefore, if all alkalinity from olivine dissolution is consumed in carbonate precipitation, half of the CO₂ is sequestered compared to a situation without carbonate precipitation. [b]fayalite weathering and sulfate reduction each produce 2 moles of alkalinity per mole of iron (Fe²⁺) and SO₄²⁻, respectively. When both Fe²⁺ and sulfide (H₂S) precipitate to form iron sulfide (FeS), 2 moles alkalinity are consumed. Thus, the net result is that 2 moles of alkalinity produced by fayalite weathering are maintained.

	Reaction mechanism	μ_{SR}
Carbonate precipitation	$Ca^{2+} + 2HCO_3^- \rightarrow CaCO_3 + CO_2 + H_2O$	1[a]
Iron oxide precipitation	$Fe^{2+} + \frac{1}{4}O_2 + 2OH^- + \frac{1}{2}H_2O \rightarrow Fe(OH)_3$	$1 \cdot x_{FAY}$
Sulfate reduction + iron sulfide precipitation	$2CH_2O + SO_4^{2-} \rightarrow 2CO_2 + H_2S + 2OH^-$ $Fe^{2+} + H_2S + 2OH^- \rightarrow FeS + 2H_2O$	$0^b \cdot x_{FAY}$

3.3.1 Stimulated precipitation and inhibited dissolution of carbonates

Carbonate precipitation consumes 1 mol of dissolved inorganic carbon (DIC) and 2 moles of alkalinity (Table 4), hence leading to the outgassing of CO₂ to the atmosphere (Wolf-Gladrow et al., 2007). In theory, different carbonate minerals can form. Given the release of Mg²⁺ and Fe²⁺ during olivine dissolution, the formation of magnesite (MgCO₃) and siderite (FeCO₃) needs consideration. However, MgCO₃ is unlikely to form during CESW in coastal sediments, as it typically only precipitates at elevated CO₂ pressure or temperature (60–100°C) (Griffioen, 2017; Saldi et al., 2009). Likewise, the formation of FeCO₃ requires particular environmental conditions, including anoxic but hydrogen sulfide (H₂S) free conditions with high concentrations of Fe²⁺ and a narrow pH window between 6.0 and 7.2 (Lin et al., 2020). Therefore, the most likely carbonates to precipitate are calcium carbonates (CaCO₃). Coastal waters are oversaturated with respect to CaCO₃ (Morse et al., 2007), and so there is concern that the addition of alkalinity through OAE could induce precipitation of the mineral (Hartmann et al., 2023; Moras et al., 2022).

The saturations state with respect to CaCO$_3$ is highly dependent on the type of sediment. In more permeable, sandy sediments, oxic respiration processes lower the pH and can result in undersaturation and dissolution of CaCO$_3$ (Milliman and Droxler, 1996; Morse and Mackenzie, 1990; Rao et al., 2014). In cohesive sediments, anoxic respiration processes produce alkalinity

640 and can elevate the saturation state of CaCO$_3$ (Berner, 1984; Turchyn et al., 2021). However, a high saturation state does not necessarily lead to CaCO$_3$ precipitation due to inhibitors such as phosphate and organic matter in the sediment (Morse et al., 2007; Turchyn et al., 2021). Flushing of the sediment through advection or bioirrigation also prevents alkalinity from building up (Rao et al., 2012).

Olivine dissolution experiments in seawater have generated mixed and conflicting results regarding the importance of
645 secondary CaCO$_3$ formation. In some experiments, CaCO$_3$ formation was observed (Fuhr et al., 2022; Rigopoulos et al., 2018), while other experiments did not show any precipitation (Bach, 2024; Flipkens et al., 2023b; Montserrat et al., 2017). One factor causing CaCO$_3$ precipitation could be that the seawater was isolated from the atmosphere in some experiments (Fuhr et al., 2022; Rigopoulos et al., 2018), whereas no precipitation was observed in experiments where gas exchange was allowed (Flipkens et al., 2023b; Montserrat et al., 2017). The latter ensures that CO$_2$ can move into solution as alkalinity is produced,
650 thus preventing a pH rise and resulting CaCO$_3$ oversaturation. Another explanation for the varying results could be the use of different types of seawater in the experiments. The presence of phosphate may have inhibited CaCO$_3$ formation in experiments with natural seawater (Bach, 2024; Flipkens et al., 2023b; Montserrat et al., 2017), in contrast to experiments conducted with phosphate-free artificial seawater (Fuhr et al., 2022; Rigopoulos et al., 2018). As predicted by thermodynamic modeling (Griffioen, 2017), no magnesite (MgCO$_3$) has been detected in olivine dissolution experiments in seawater (Flipkens et al.,
655 2023b; Fuhr et al., 2022; Montserrat et al., 2017; Rigopoulos et al., 2018). Siderite (FeCO$_3$) formation was not explicitly investigated in the experiments, but as noted above, this process is unlikely based on theoretical grounds.

Although CESW may not cause precipitation of CaCO$_3$ in the sediment, it could impede natural alkalinity production by inhibiting the dissolution of CaCO$_3$ already present in the sediment (Bach, 2024). As such, the alkalinity sourced from carbonate dissolution is substituted with alkalinity from olivine dissolution, so the alkalinity generated by CESW is no longer
660 fully additional to the alkalinity efflux before CESW application. While the additionality problem may imply that CESW does not increase the sedimentary alkalinity release, the CO$_2$ sequestration potential still increases when alkalinity originates from olivine, as CaCO$_3$ dissolution results in a concomitant release of alkalinity and DIC, while no DIC is produced during olivine dissolution. The additionality problem may be an issue for CESW in both the permeable and cohesive sediment application scenarios (Fig. 2c–d), in which the dissolution of olivine dissolution occurs at the location of carbonate dissolution. It should
665 however not affect the bedload application (Fig. 2b), as the olivine is weathering in seawater that is already oversaturated with respect to CaCO$_3$, and there is also an immediate dilution of the alkalinity. In conclusion, the rate at which CESW applications influence natural alkalinity release from sediments imposes a major uncertainty on μ_{SR}. The additionality problem could have profound implications for the location chosen for CESW application and the economics and MRV of a CESW project, as the net alkalinity generation must be quantified rather than the total sedimentary alkalinity release. Hence, future CESW

670 experiments need to quantify the natural alkalinity production in control sediments and determine to what extent this process is affected by mineral addition.

A final concern about OAE relates to strong alkalinity excursions in the overlying water leading to the precipitation of carbonates. While CESW targets a slow release of alkalinity from the sediment, other OAE approaches (Fig. 1b), such as ocean liming and electrochemistry, target a fast, immediate release of alkalinity. These fast-release approaches can result in

675 substantial alkalinity increases at the local scale. In recent liming experiments, the addition of ~250 µmol kg^{-1} alkalinity on top of a seawater baseline of 2400 µmol kg^{-1} (a ~10% increase, equivalent to an aragonite saturation index of ~5) was delineated as a safe threshold to avoid CaCO$_3$ precipitation in the water (Moras et al., 2022). In contrast, the addition of 500 µmol kg^{-1} of alkalinity led to "runaway precipitation", a process where CaCO$_3$ precipitation continued until the aragonite saturation reached 1.8–2.0 and the alkalinity concentration had been reduced below the initial seawater values (Hartmann et al., 2023; Moras et

680 al., 2022). The slow alkalinity release from the seabed during CESW implies a substantial dilution in the overlying water, thus avoiding local alkalinity excursions, and hence the chances of immediate CaCO$_3$ precipitation in the overlying water are minimal.

3.3.2 Iron mineral formation

Dissolution of fayalite releases Fe^{2+} to the pore water, which in oxic environments spontaneously precipitates as iron

685 (hydr)oxides during aerobic oxidation (Griffioen, 2017). Iron oxidation consumes 2 moles of alkalinity per mole of Fe^{2+}, equaling the alkalinity produced during fayalite dissolution. Olivine consists of 6–20 mol% Fe (Ackerman et al., 2009; Deer et al., 2013; Harben and Smith, 2006; Rehfeldt et al., 2007; Su et al., 2016), thus providing a μ_{SR} of 0.06–0.20 if all Fe^{2+} becomes oxidized. The formation of iron (hydr)oxides has been confirmed in olivine dissolution experiments in seawater (Fuhr et al., 2022; Rigopoulos et al., 2018). Precipitation of iron (hydr)oxides is also expected from a thermodynamic perspective,

690 as these experiments were conducted under well-oxygenated conditions. During CESW applications, well-flushed and well-oxygenated sediments are targeted to avoid porewater saturation effects, so the alkalinity reduction due to Fe oxidation from fayalite needs consideration.

If olivine particles are buried in deeper, anoxic sediment layers, the Fe^{2+} released from fayalite dissolution can react with H$_2$S and form iron sulfides (FeS$_x$, Table 4). Like iron oxide formation, the precipitation of the FeS$_x$ consumes the alkalinity formed

695 through fayalite dissolution. However, the alkalinity formed via sulfate reduction is preserved when H$_2$S is prevented from reoxidizing through trapping in the sediment (Hu and Cai, 2011; Middelburg et al., 2020), causing a net alkalinity production of 4 mol per mol olivine and thus giving a μ_{SR} of 0. However, the fate of any FeS$_x$ minerals produced must be closely scrutinized, as it will determine the permanence of the alkalinity produced. If the FeS$_x$ comes into contact with O$_2$ (e.g. through bioirrigation or physical advection), they will be reoxidized, and the alkalinity produced during their precipitation will be

700 consumed again (Schippers and Jørgensen, 2002). The long-term fate of ferrous iron released during CESW trials is not well constrained, and will most likely, strongly depend on the application scenario (cohesive versus permeable). It is hence an important point of attention in future mesocosm experiments and field trials.

3.4 The CO₂ sequestration efficiency

The final step in the CESW process represents the equilibration of CO_2 at the air-sea interface (Fig. 2). This air-sea CO_2
705 exchange does not occur immediately but typically takes place on a time scale of months up to a year, with longer timescales
associated with deep mixed layers (Jones et al., 2014). The amount of CO_2 that will be eventually captured from the atmosphere
by the addition of alkalinity is given by the CO_2 sequestration efficiency ρ_{CO_2}, which is a thermodynamic quantity defined as
(Zeebe and Wolf-Gladrow, 2001):

$$\rho_{CO_2} = \left(\frac{\partial DIC}{\partial A_T} \right)_{f_{CO_2}} \tag{13}$$

710 This partial derivative represents the change in the concentration of DIC upon the addition of one mole of alkalinity (A_T) to
the seawater, evaluated at a constant fugacity (or partial pressure) of CO_2 (f_{CO_2}) (Wolf-Gladrow et al., 2007; Bertagni and
Porporato, 2022). The value of ρ_{CO_2} can be calculated using dedicated software packages for seawater carbonate chemistry
like AquaEnv (Hofmann et al., 2009) or CO2sys (Xu et al., 2017).

The magnitude of ρ_{CO_2} depends on the local seawater chemistry, temperature, and salinity, causing ρ_{CO_2} to vary between
715 different coastal systems (Middelburg et al., 2020; Bertagni and Porporato, 2022). Across the global ocean, ρ_{CO_2} ranges from
~0.75–0.95 with an average value of 0.84 (Bertagni and Porporato, 2022; Schulz et al., 2023). Figure 6a displays the predicted
DIC as a function of alkalinity for a set of endmember conditions for salinity and temperature relevant to coastal systems. This
graph illustrates the key mechanism underlying OAE: an increase in the alkalinity of seawater leads to an increase in DIC after
equilibration with the atmosphere. The slope of the lines depict ρ_{CO_2} (Bertagni and Porporato, 2022; Schulz et al., 2023),
720 which depends on temperature, salinity, and local seawater chemistry. Colder and less saline waters can store more CO_2 (Zeebe
and Wolf-Gladrow, 2001) and are characterized by a higher ρ_{CO_2} (Fig. 6a). Figure 6b–d illustrate the impact of local seawater
chemistry (i.e., as specified by pH and f_{CO_2}), temperature, and salinity on ρ_{CO_2}. As a reference condition, we use pH = 8.07
(all pH values presented are on the total pH scale), temperature = 15°C, salinity = 35, and current CO_2 levels (f_{CO_2} = 420
ppm).

725 The surface ocean pH between 60°N to 60°S varies between 8.0 and 8.25, with a global average of 8.07 ± 0.02 (Jiang et al.,
2019). In coastal areas, riverine input can cause larger variations in the pH, since the pH of rivers typically ranges between 6
and 8 (Mackenzie and Lerman, 2006). As shown in Fig. 6b, theoretically, the pH exerts a strong influence on ρ_{CO_2} when
moving across the entire pH scale from 4 to 12. At pH <5, ρ_{CO_2} effectively becomes zero since the addition of alkalinity here
leads to a consumption of H⁺ rather than the production of HCO_3^- or CO_3^{2-}, and hence there is no scavenging of CO_2 (Bertagni
730 and Porporato, 2022; Hofmann et al., 2008). At higher pH, ρ_{CO_2} increases to a maximum value of 0.97 at pH = 6.7, before
decreasing again beyond pH ~8 and stabilizing at $\rho_{CO_2} \approx 0.5$ at pH > 10. Note that the value of $\rho_{CO_2} = 1$ is never reached in
seawater due to the presence of the borate buffer (Bertagni and Porporato, 2022). When considering the typical current ocean
seawater pH range of 8.0–8.25, the ρ_{CO_2} variation is minimal with values of 0.83-0.88 (Fig. 6b).
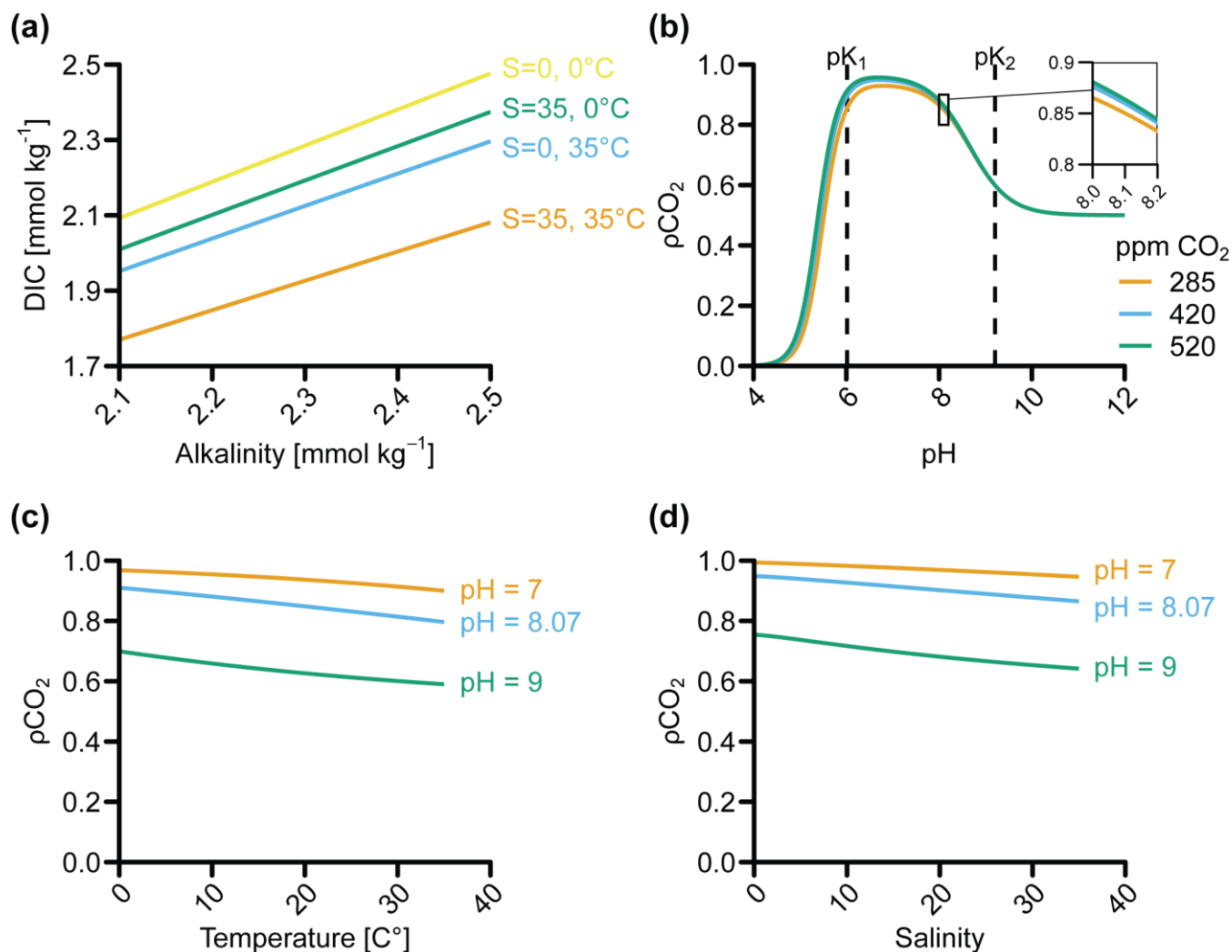
Figure 6. The CO_2 sequestration efficiency (ρ_{CO_2}) as a function of environmental parameters (unless otherwise stated pH = 8.07, temperature = 15 °C, salinity = 35, f_{CO_2} = 420 ppm). (a) Predicted DIC as a function of alkalinity for a set of endmember temperature and salinity values. (b) ρ_{CO_2} as a function of pH at different levels of atmospheric CO_2 (constant temperature and salinity), with pK values from Lueker et al. (2000). Typical seawater pH is shown in magnification. (c) ρ_{CO_2} as a function of temperature at different pH levels (constant salinity and f_{CO_2}).

Temperature and salinity influence ρ_{CO_2} through the stoichiometric equilibrium constants (K^*) of the carbonate system: ρ_{CO_2} decreases with increasing temperature (Fig. 6c) and increasing salinity (Fig. 6d). The temperature effect is in large part due to the presence of a borate buffer in seawater, which also contributes to alkalinity. An increase in temperature decreases the solubility of CO_2 without affecting the borate concentration, leading to a decreasing ratio between DIC and borate (Bertagni and Porporato, 2022). Across the ocean, the temperature varies between 0 and 35°C (Sarmiento and Gruber, 2006), which results in a ρ_{CO_2} range from 0.80 to 0.91 (Fig. 6c).

The effect of salinity on ρ_{CO_2} is driven by ion activity. When the salinity (and hence the number of ions in solution) increases, the ion activity decreases. Since the activities of different ions are not affected by the same magnitude, the ratio of their activity coefficients changes. For the carbonate system, the activity coefficient of the bivalent CO_3^{2-} decreases more rapidly with increasing salinity than those of the monovalent ions HCO_3^- and H^+. A decrease in salinity thus shifts the entire ρ_{CO_2} curve to the left (Fig. 6a). The impact of salinity on ρ_{CO_2} in the open ocean is minimal, as the variation in surface salinity is in the range 33–37 (Sarmiento and Gruber, 2006), giving a ρ_{CO_2} difference of <0.01 (Fig. 6d). In estuaries, however, the salinity can vary from 0–35, which implies a decrease in ρ_{CO_2} from 0.95 to 0.86.

The atmospheric CO_2 concentration also affects ρ_{CO_2}. When atmospheric CO_2 levels increase, more CO_2 moves into solution to maintain the equilibrium between water and air, as described by Le Chatelier's principle. An increase in the atmospheric CO_2 concentration of 100 ppm would increase ρ_{CO_2} by ~0.004.

4 Conclusions and future outlook

CDR technologies are urgently required to meet the targets of the Paris Climate Agreement, and OAE through CESW is considered a promising candidate (Meysman and Montserrat, 2017). A considerable advantage of CESW is the possibility of rapid deployment and scalability, as no new technologies need to be developed. Since CESW mimics the natural process of chemical rock weathering (Fig. 1), its theoretical underpinnings are well understood: when fine-grained silicates are added to coastal sediment environments, they remain out of thermodynamic equilibrium and will dissolve, thus releasing alkalinity (Fig. 2). Although mining efforts would have to be substantially expanded to supply olivine for CESW, potential dunite reserves are large, so resource availability does not appear to be a limiting factor. Furthermore, the deposition of olivine onto the seafloor is expected to increase the dissolution rate of olivine by exposing it to the benthic weathering engine: chemical weathering can be enhanced by wave-induced physical abrasion, removal of weathering products through advection and bioirrigation, and exposure to a lower pH (compared to the overlying water). Although initial studies are positive (Flipkens et al., 2023b), the efficiency of this benthic weathering engine under relevant natural conditions remains poorly quantified, and so this is an important point of attention for future CESW studies.

Coastal environments are geochemically complex and heterogeneous, so the practical implementation of CESW requires consideration of many processes, some of which are still poorly constrained (e.g. the impact of saturation effects in the pore water in different types of coastal sediments). Moreover, the intrinsic geochemical difference between various types of coastal sediments (e.g. cohesive versus permeable CESW application) has been given very little attention. In addition, much of our current understanding of the efficiency of CESW is based on idealized laboratory experiments in aqueous solutions water with high fluid-to-mineral ratios, and it is unknown to what extent these results can be extrapolated to natural CESW field sites. Here, we have provided a systematic review of the parameters that determine the CO_2 sequestration rate of olivine-based CESW (Table 5) and have identified aspects that need consideration when applying CESW in actual coastal environments.

Table 5 Summary of predictability of each parameter needed to calculate the CO₂ sequestration rate from CESW (basis for classification in supplementary file 1.3).

Parameter	Symbol	Predictability
CO₂ sequestration efficiency	ρ_{CO_2}	High
Molar mass olivine	$M_{olivine}$	High
Mass fraction of inert minerals	x_{inert}	High
Intrinsic olivine dissolution rate	k_d	Moderate
Specific surface area	A_{surf}	Moderate
Stoichiometric alkalinity production factor	γ_{A_T}	Moderate
Secondary reactions	μ_{SR}	Low
Saturation factor	Ω	Low

780

Table 5 lists the parameters that affect the dissolution of olivine and the associated CO_2 sequestration efficiency and provides an assessment of their current predictability (i.e. how well we can predict them for a given environment with current knowledge). The parameters ρ_{CO_2}, x_{inert}, and $M_{olivine}$ are classified as "highly predictable" as they can either be calculated from environmental data (ρ_{CO_2}) or can be accurately derived by chemical analysis of the source rock of olivine (x_{inert} and

785    $M_{olivine}$). In contrast, the prediction of the dissolution rate of olivine in actual coastal sediments is hampered by several uncertainties, and so the predictability of the associated parameters k_d, A_{surf}, and γ_{A_T} is qualified as "moderate". The value of k_d is well-studied in laboratory settings, but its actual value within actual marine sediments bears considerable uncertainty. Experiments with a particular focus on CESW are typically conducted in laboratory reactors with high fluid-to-sediment ratios. No information on k_d within actual sediments is available, which makes it difficult to estimate k_d for the three suggested

790   CESW application scenarios (bedload, permeable, and cohesive sediment applications). Therefore, attaining estimates of k_d in these different natural sediment settings should be a research priority. As pH is a critical parameter in determining k_d, an improved understanding of pore water pH as a function of sediment type would be beneficial in assessing which application sites are promising for CESW. Furthermore, a more detailed and systematic monitoring of A_{surf} seems adamant. A_{surf} is typically only measured or reported before the start of dissolution experiments; measurement of A_{surf} and R_S throughout

795   (long-term) applications could give important information on how A_{surf} changes during CESW application. With regards to γ_{A_T}, the formation of sepiolite and serpentine seems unlikely in coastal sediment conditions. However, this has not been investigated for CESW in actual sediments. Additionally, the formation of clay minerals (e.g. iddingsite) has not been extensively addressed.

Another important parameter governing olivine dissolution is Ω, for which very little data is currently available. The

800   predictability of Ω is qualified as "low". This uncertainty relates to the residence time of the pore water, which is determined by an intricate interplay between the grain size and properties of the ambient sediment, the local hydrodynamics, and the benthic fauna community composition. It seems imperative to CESW that olivine is applied to well-flushed sediments so that

alkalinity and weathering products do not accumulate (hence $\Omega \ll 1$). Furthermore, initial experiments suggest a low likelihood of passivating layer formation on olivine surfaces in well-flushed environments. The development of such layers
805   may further be prevented by physical abrasion and passing through the guts of animals in natural sediment conditions. The predictability of μ_{SR} is qualified as "low".

The production of alkalinity in the sediment through olivine dissolution does not imply that this alkalinity will also reach the overlying water column and therefore emerges as an important point of attention. At present, we have a restricted understanding of the relation between olivine dissolution and carbonate precipitation and dissolution in natural sediments. Initial studies
810   suggest that induced carbonate precipitation is limited, and the risk of runaway precipitation (in the sediment or water) is low since alkalinity is released slowly during CESW and added to an extensive volume of water. However, there is currently considerable uncertainty around how CESW would impact natural carbonate dissolution within the sediment and whether CESW-generated alkalinity is fully additive to the natural alkalinity generation (Bach, 2024).

Overall, we conclude that while studies show a clear potential for CESW as a CDR method, future experiments should focus
815   on improved quantification of olivine dissolution rates as well as alkalinity release rates in actual sediment environments. There is hence a clear need for *in situ* field trials, which are essential to quantify how efficiently CESW performs as an OAE technology. Before field trials are launched, microcosm and mesocosm experiments with natural sediment are crucial to increase the predictability of CESW effects. Both alkalinity effluxes from the sediment as well as the chemical conditions in the pore water before and after the application of olivine should be monitored. Since the effect of CESW is expected to vary
820   seasonally, measurements should have a sufficiently high temporal resolution to allow trends to be quantified for MRV. Olivine grains should further be recovered throughout experiments to verify olivine dissolution features, formation of passivating layers, and occurrence of secondary precipitation reactions. Detailed evaluations of the ecotoxicological and environmental impacts of CESW are another prerequisite for field trials. Accordingly, a critical next step for CESW is to determine the efficacy of CO_2 drawdown in real-life conditions and its impacts on the broader environment. Moreover, the outcome of these
825   field experiments will determine MRV protocols, which need to be designed and agreed upon, so that CESW applications can proceed in a sustainable and economically feasible manner.

Author contribution

LG was responsible for formal analysis, data collection, visualization, and writing of the original draft. LG and FJRM were responsible for the conceptualization. FJRM conceived and supervised the study. LG and FJRM took the lead in writing with
830   additional input from AH. All authors discussed the results and contributed to the final manuscript.

Competing interests

The authors declare that they have no conflict of interest.

Financial support

LG was supported by a PhD fellowship from the Research Foundation – Flanders (FWO) (project number 1S08321N). AH
835 was supported by a junior postdoctoral fellowship from FWO (project nr 1241724N). FJRM was supported by the Strategic
Basic Research (SBO) project from FWO (project nr S000619N). This research was financially supported by Team for the
Planet (https://team-planet.com), a citizen community initiative dedicated to tackling the climate challenge (funding through
a collaboration agreement with its Carbon Time subsidiary).

Acknowledgments

840 The authors thank Sebastiaan van de Velde and Gunter Flipkens for academic discussions. Next, we would also like to thank
Vincent Sluydts for his assistance with calculating the uncertainty for the intrinsic dissolution rate constant. Ivan Communod
and Mathieu Helwig from Carbon Time are thanked for their continued support.

References

Ackerman, L., Jelínek, E., Medaris, G., Ježek, J., Siebel, W., and Strnad, L.: Geochemistry of Fe-rich peridotites and associated
845 pyroxenites from Horní Bory, Bohemian Massif: Insights into subduction-related melt–rock reactions, Chem. Geol., 259, 152–
167, https://doi.org/10.1016/j.chemgeo.2008.10.042, 2009.

Alexander, G., Mercedes Maroto-Valer, M., and Gafarova-Aksoy, P.: Evaluation of reaction variables in the dissolution of
serpentine for mineral carbonation, Fuel, 86, 273–281, https://doi.org/10.1016/j.fuel.2006.04.034, 2007.

Alt, J. C., Shanks, W. C., Crispini, L., Gaggero, L., Schwarzenbach, E. M., Früh-Green, G. L., and Bernasconi, S. M.: Uptake
850 of carbon and sulfur during seafloor serpentinization and the effects of subduction metamorphism in Ligurian peridotites,
Chem. Geol., 322–323, 268–277, https://doi.org/10.1016/j.chemgeo.2012.07.009, 2012.

Alt, J. C., Schwarzenbach, E. M., Früh-Green, G. L., Shanks, W. C., Bernasconi, S. M., Garrido, C. J., Crispini, L., Gaggero,
L., Padrón-Navarta, J. A., and Marchesi, C.: The role of serpentinites in cycling of carbon and sulfur: Seafloor serpentinization
and subduction metamorphism, Lithos, 178, 40–54, https://doi.org/10.1016/j.lithos.2012.12.006, 2013.

855 Archer, D., Eby, M., Brovkin, V., Ridgwell, A., Cao, L., Mikolajewicz, U., Caldeira, K., Matsumoto, K., Munhoven, G.,
Montenegro, A., and Tokos, K.: Atmospheric Lifetime of Fossil Fuel Carbon Dioxide, Annu. Rev. Earth Planet. Sci., 37, 117–
134, https://doi.org/10.1146/annurev.earth.031208.100206, 2009.

Bach, L. T.: The additionality problem of ocean alkalinity enhancement, Biogeosciences, 21, 261–277,
https://doi.org/10.5194/bg-21-261-2024, 2024.

860 Bach, L. T., Gill, S. J., Rickaby, R. E. M., Gore, S., and Renforth, P.: CO2 Removal With Enhanced Weathering and Ocean
Alkalinity Enhancement: Potential Risks and Co-benefits for Marine Pelagic Ecosystems, Front. Clim., 1, 2019.

Bailey, A.: Proceedings of the International Symposium on Water-Rock Interaction (eds. J. Cadek and T. Paces), in: Effects of temperature on the reaction of silicates with aqueous solutions in the low temperature range, Geological Survey Prague, Prague, 375–380, 1976.

865 Baker, I. and Haggerty, S. E.: The alteration of olivine in basaltic and associated lavas, Contrib. Mineral. Petrol., 16, 258–273, https://doi.org/10.1007/BF00371095, 1967.

Baldermann, A., Mavromatis, V., Frick, P. M., and Dietzel, M.: Effect of aqueous Si/Mg ratio and pH on the nucleation and growth of sepiolite at 25 °C, Geochim. Cosmochim. Acta, 227, 211–226, https://doi.org/10.1016/j.gca.2018.02.027, 2018.

Béarat, H., McKelvy, M. J., Chizmeshya, A. V. G., Gormley, D., Nunez, R., Carpenter, R. W., Squires, K., and Wolf, G. H.:
870 Carbon Sequestration via Aqueous Olivine Mineral Carbonation: Role of Passivating Layer Formation, Environ. Sci. Technol., 40, 4802–4808, https://doi.org/10.1021/es0523340, 2006.

Berner, R. A.: Sedimentary pyrite formation: An update, Geochim. Cosmochim. Acta, 48, 605–615, https://doi.org/10.1016/0016-7037(84)90089-9, 1984.

Berner, R. A.: The Phanerozoic Carbon Cycle: CO2 and O2, 1st ed., Oxford University Press, USA, 2004.

875 Berner, R. A., Lasaga, A. C., and Garrels, R. M.: The carbonate-silicate geochemical cycle and its effect on atmospheric carbon dioxide over the past 100 million years, Am. J. Sci., 283, 641–683, https://doi.org/10.2475/ajs.283.7.641, 1983.

Bertagni, M. B. and Porporato, A.: The Carbon-Capture Efficiency of Natural Water Alkalinization: Implications For Enhanced weathering, Sci. Total Environ., 838, 156524, https://doi.org/10.1016/j.scitotenv.2022.156524, 2022.

Blum, A. and Lasaga, A.: Role of surface speciation in the low-temperature dissolution of minerals, Nature, 331, 431–433,
880 https://doi.org/10.1038/331431a0, 1988.

Brantley, S. L. and Mellott, N. P.: Surface area and porosity of primary silicate minerals, Am. Mineral., 85, 1767–1783, https://doi.org/10.2138/am-2000-11-1220, 2000.

Brantley, S. L., Kubicki, J. D., and White, A. F. (Eds.): Kinetics of water-rock interaction, Springer Verlag, New York, 833 pp., 2008.

885 Brown, G. and Stephen, I.: A Structural study of iddingsite from New South Wales, Australia, Am. Mineral., 44, 251–260, 1959.

Brunauer, S., Emmett, P. H., and Teller, E.: Adsorption of Gases in Multimolecular Layers, J. Am. Chem. Soc., 60, 309–319, https://doi.org/10.1021/ja01269a023, 1938.

Bucher, K. and Grapes, R.: Metamorphism of Ultramafic Rocks, in: Petrogenesis of Metamorphic Rocks, edited by: Bucher,
890 K. and Grapes, R., Springer, Berlin, Heidelberg, 191–224, https://doi.org/10.1007/978-3-540-74169-5_5, 2011.

Bullock, L. A., James, R. H., Matter, J., Renforth, P., and Teagle, D. A. H.: Global Carbon Dioxide Removal Potential of Waste Materials From Metal and Diamond Mining, Front. Clim., 0, https://doi.org/10.3389/fclim.2021.694175, 2021.

Cai, W.-J., Reimers, C. E., and Shaw, T.: Microelectrode studies of organic carbon degradation and calcite dissolution at a California Continental rise site, Geochim. Cosmochim. Acta, 59, 497–511, https://doi.org/10.1016/0016-7037(95)00316-R,
895 1995.

Campbell, J. S., Foteinis, S., Furey, V., Hawrot, O., Pike, D., Aeschlimann, S., Maesano, C. N., Reginato, P. L., Goodwin, D. R., Looger, L. L., Boyden, E. S., and Renforth, P.: Geochemical Negative Emissions Technologies: Part I. Review, Front. Clim., 4, 2022.

900 Caserini, S., Storni, N., and Grosso, M.: The Availability of Limestone and Other Raw Materials for Ocean Alkalinity Enhancement, Glob. Biogeochem. Cycles, 36, e2021GB007246, https://doi.org/10.1029/2021GB007246, 2022.

Casey, W. H. and Sposito, G.: On the temperature dependence of mineral dissolution rates, Geochim. Cosmochim. Acta, 56, 3825–3830, https://doi.org/10.1016/0016-7037(92)90173-G, 1992.

Chen, Y. and Brantley, S. L.: Dissolution of forsteritic olivine at 65°C and 2, Chem. Geol., 165, 267–281, https://doi.org/10.1016/S0009-2541(99)00177-1, 2000.

905 Corner, A. and Pidgeon, N.: Like artificial trees? The effect of framing by natural analogy on public perceptions of geoengineering, Clim. Change, 130, 425–438, https://doi.org/10.1007/s10584-014-1148-6, 2015.

Crundwell, F. K.: The mechanism of dissolution of forsterite, olivine and minerals of the orthosilicate group, Hydrometallurgy, 150, 68–82, https://doi.org/10.1016/j.hydromet.2014.09.006, 2014.

Cyronak, T., Albright, R., and Bach, L. T.: Field experiments in ocean alkalinity enhancement research, State Planet, 2-
910 oae2023, 1–13, https://doi.org/10.5194/sp-2-oae2023-7-2023, 2023.

Daval, D., Sissmann, O., Menguy, N., Saldi, G. D., Guyot, F., Martinez, I., Corvisier, J., Garcia, B., Machouk, I., Knauss, K. G., and Hellmann, R.: Influence of amorphous silica layer formation on the dissolution rate of olivine at 90°C and elevated pCO2, Chem. Geol., 284, 193–209, https://doi.org/10.1016/j.chemgeo.2011.02.021, 2011.

Deer, W. A., Howie, R. A., and Zussman, J.: Olivine, in: An Introduction to the Rock-Forming Minerals, 4–11, 2013.

915 Delvigne, J., Bisdom, E. B. A., Sleeman, J., and Stoops, G.: Olivines, their pseudomorphs and secondary products, 63, 1979.

Dichicco, M. C., Laurita, S., Paternoster, M., Rizzo, G., Sinisi, R., and Mongelli, G.: Serpentinite Carbonation for CO2 Sequestration in the Southern Apennines: Preliminary Study, Energy Procedia, 76, 477–486, https://doi.org/10.1016/j.egypro.2015.07.888, 2015.

Dickson, A. G.: pH scales and proton-transfer reactions in saline media such as sea water, Geochim. Cosmochim. Acta, 48,
920 2299–2308, https://doi.org/10.1016/0016-7037(84)90225-4, 1984.

Edwards, A. B.: The Formation of Iddingsite, Am. Mineral., 23, 277–281, 1938.

Eggleton, R. A.: Formation of Iddingsite Rims on Olivine: A Transmission Electron Microscopy Study, Clays Clay Miner., 32, 1–11, https://doi.org/10.1346/CCMN.1984.0320101, 1984.

Eriksson, E.: On the rate of dissolution of olivine in aqueous solutions, Vatten, 38, 409–415, 1982.

925 Farhang, F., Rayson, M., Brent, G., Hodgins, T., Stockenhuber, M., and Kennedy, E.: Insights into the dissolution kinetics of thermally activated serpentine for CO2 sequestration, Chem. Eng. J., 330, 1174–1186, https://doi.org/10.1016/j.cej.2017.08.073, 2017.

Flipkens, G., Blust, R., and Town, R. M.: Deriving Nickel (Ni(II)) and Chromium (Cr(III)) Based Environmentally Safe Olivine Guidelines for Coastal Enhanced Silicate Weathering, Environ. Sci. Technol., https://doi.org/10.1021/acs.est.1c02974, 2021.

930

Flipkens, G., Horoba, K., Bostyn, K., Geerts, L. J. J., Town, R. M., and Blust, R.: Acute bioaccumulation and chronic toxicity of olivine in the marine amphipod Gammarus locusta, Aquat. Toxicol., 106662, https://doi.org/10.1016/j.aquatox.2023.106662, 2023a.

Flipkens, G., Fuhr, M., Fiers, G., Meysman, F. J. R., Town, R. M., and Blust, R.: Enhanced olivine dissolution in seawater

935 through continuous grain collisions, Geochim. Cosmochim. Acta, 359, 84–99, https://doi.org/10.1016/j.gca.2023.09.002, 2023b.

Foteinis, S., Campbell, J. S., and Renforth, P.: Life Cycle Assessment of Coastal Enhanced Weathering for Carbon Dioxide Removal from Air, Environ. Sci. Technol., https://doi.org/10.1021/acs.est.2c08633, 2023.

Fuhr, M., Geilert, S., Schmidt, M., Liebetrau, V., Vogt, C., Ledwig, B., and Wallmann, K.: Kinetics of Olivine Weathering in

940 Seawater: An Experimental Study, Front. Clim., 4, https://doi.org/10.3389/fclim.2022.831587, 2022.

Fuhr, M., Wallmann, K., Dale, A. W., Diercks, I., Kalapurakkal, H. T., Schmidt, M., Sommer, S., Böhnke, S., Perner, M., and Geilert, S.: Disentangling artificial and natural benthic weathering in organic rich Baltic Sea sediments, Front. Clim., 5, https://doi.org/10.3389/fclim.2023.1245580, 2023.

Fuss, S., Lamb, W. F., Callaghan, M. W., Hilaire, J., Creutzig, F., Amann, T., Beringer, T., Garcia, W. de O., Hartmann, J.,

945 Khanna, T., Luderer, G., Nemet, G. F., Rogelj, J., Smith, P., Vicente, J. L. V., Wilcox, J., Dominguez, M. del M. Z., and Minx, J. C.: Negative emissions—Part 2: Costs, potentials and side effects, Environ. Res. Lett., 13, 063002, https://doi.org/10.1088/1748-9326/aabf9f, 2018.

Gaudin, A., Dehouck, E., Grauby, O., and Mangold, N.: Formation of clay minerals on Mars: Insights from long-term experimental weathering of olivine, Icarus, 311, 210–223, https://doi.org/10.1016/j.icarus.2018.01.029, 2018.

950 Gerrits, R., Pokharel, R., Breitenbach, R., Radnik, J., Feldmann, I., Schuessler, J. A., von Blanckenburg, F., Gorbushina, A. A., and Schott, J.: How the rock-inhabiting fungus *K. petricola* A95 enhances olivine dissolution through attachment, Geochim. Cosmochim. Acta, 282, 76–97, https://doi.org/10.1016/j.gca.2020.05.010, 2020.

Gerrits, R., Wirth, R., Schreiber, A., Feldmann, I., Knabe, N., Schott, J., Benning, L. G., and Gorbushina, A. A.: High-resolution imaging of fungal biofilm-induced olivine weathering, Chem. Geol., 559, 119902,

955 https://doi.org/10.1016/j.chemgeo.2020.119902, 2021.

Giammar, D. E., Bruant, R. G., and Peters, C. A.: Forsterite dissolution and magnesite precipitation at conditions relevant for deep saline aquifer storage and sequestration of carbon dioxide, Chem. Geol., 217, 257–276, https://doi.org/10.1016/j.chemgeo.2004.12.013, 2005.

Goff, F. and Lackner, K. S.: Carbon Dioxide Sequestering Using Ultramaf ic Rocks, Environ. Geosci., 5, 89–102,

960 https://doi.org/10.1046/j.1526-0984.1998.08014.x, 1998.

Goff, F., Guthrie, G., Lipin, B., Fite, M., Chipera, S., Counce, D., Kluk, E., and Ziock, H.: Evaluation of ultramafic deposits in the Eastern United States and Puerto Rico as sources of magnesium for carbon dioxide sequestration, Los Alamos National Lab. (LANL), Los Alamos, NM (United States), https://doi.org/10.2172/754045, 2000.

965   Golubev, S. V., Pokrovsky, O. S., and Schott, J.: Experimental determination of the effect of dissolved CO2 on the dissolution kinetics of Mg and Ca silicates at 25 °C, Chem. Geol., 217, 227–238, https://doi.org/10.1016/j.chemgeo.2004.12.011, 2005.

Grandstaff, D. E.: Changes in surface area and morphology and the mechanism of forsterite dissolution, Geochim. Cosmochim. Acta, 42, 1899–1901, https://doi.org/10.1016/0016-7037(78)90245-4, 1978.

Grandstaff, D. E.: The dissolution rate of forsteritic olivine from Hawaiian beach sand, in: Rates of Chemical Weathering of Rocks and Minerals, edited by: Colman, S. M. and Dethier, D. P., Academic Press, 41–57, 1986.

970   Griffioen, J.: Enhanced weathering of olivine in seawater: The efficiency as revealed by thermodynamic scenario analysis, Sci. Total Environ., 575, 536–544, https://doi.org/10.1016/j.scitotenv.2016.09.008, 2017.

Hänchen, M., Prigiobbe, V., Storti, G., Seward, T. M., and Mazzotti, M.: Dissolution kinetics of fosteritic olivine at 90–150°C including effects of the presence of CO2, Geochim. Cosmochim. Acta, 70, 4403–4416, https://doi.org/10.1016/j.gca.2006.06.1560, 2006.

975   Hänchen, M., Krevor, S., Mazzotti, M., and Lackner, K. S.: Validation of a population balance model for olivine dissolution, Chem. Eng. Sci., 62, 6412–6422, https://doi.org/10.1016/j.ces.2007.07.065, 2007.

Hangx, S. J. T. and Spiers, C. J.: Coastal spreading of olivine to control atmospheric CO2 concentrations: A critical analysis of viability, Int. J. Greenh. Gas Control, 3, 757–767, https://doi.org/10.1016/j.ijggc.2009.07.001, 2009.

Harben, P. W. and Smith, C., Jr.: Olivine, in: Industrial minerals & rocks: commodities, markets, and uses, edited by: Kogel, J. E., Trivedi, N. C., Barker, J. M., and Krukowski, S. T., SME, Littleton, Colo., 679–683, 2006.

980   Hartmann, J., West, A. J., Renforth, P., Köhler, P., Rocha, C. L. D. L., Wolf-Gladrow, D. A., Dürr, H. H., and Scheffran, J.: Enhanced chemical weathering as a geoengineering strategy to reduce atmospheric carbon dioxide, supply nutrients, and mitigate ocean acidification, Rev. Geophys., 51, 113–149, https://doi.org/10.1002/rog.20004, 2013.

Hartmann, J., Suitner, N., Lim, C., Schneider, J., Marín-Samper, L., Arístegui, J., Renforth, P., Taucher, J., and Riebesell, U.: Stability of alkalinity in ocean alkalinity enhancement (OAE) approaches – consequences for durability of CO_2 storage, Biogeosciences, 20, 781–802, https://doi.org/10.5194/bg-20-781-2023, 2023.

985   Harvey, L. D. D.: Mitigating the atmospheric CO2 increase and ocean acidification by adding limestone powder to upwelling regions, J. Geophys. Res. Oceans, 113, https://doi.org/10.1029/2007JC004373, 2008.

Hausrath, E. M. and Brantley, S. L.: Basalt and olivine dissolution under cold, salty, and acidic conditions: What can we learn about recent aqueous weathering on Mars?, J. Geophys. Res. Planets, 115, https://doi.org/10.1029/2010JE003610, 2010.

990   Hellmann, R., Wirth, R., Daval, D., Barnes, J.-P., Penisson, J.-M., Tisserand, D., Epicier, T., Florin, B., and Hervig, R. L.: Unifying natural and laboratory chemical weathering with interfacial dissolution–reprecipitation: A study based on the nanometer-scale chemistry of fluid–silicate interfaces, Chem. Geol., 294–295, 203–216, https://doi.org/10.1016/j.chemgeo.2011.12.002, 2012.

995 Heřmanská, M., Voigt, M. J., Marieni, C., Declercq, J., and Oelkers, E. H.: A comprehensive and internally consistent mineral dissolution rate database: Part I: Primary silicate minerals and glasses, Chem. Geol., 597, 120807, https://doi.org/10.1016/j.chemgeo.2022.120807, 2022.

Hofmann, A. F., Meysman, F. J. R., Soetaert, K., and Middelburg, J. J.: A step-by-step procedure for pH model construction in aquatic systems, 25, https://doi.org/10.5194/bg-5-227-2008, 2008.

1000 Hofmann, A. F., Middelburg, J. J., Soetaert, K., and Meysman, F. J. R.: pH modelling in aquatic systems with time-variable acid-base dissociation constants applied to the turbid, tidal Scheldt estuary, Biogeosciences, 6, 1539–1561, https://doi.org/10.5194/bg-6-1539-2009, 2009.

Hu, X. and Cai, W.-J.: An assessment of ocean margin anaerobic processes on oceanic alkalinity budget, Glob. Biogeochem. Cycles, 25, https://doi.org/10.1029/2010GB003859, 2011.

1005 Huijgen, W. J. J., Witkamp, G.-J., and Comans, R. N. J.: Mechanisms of aqueous wollastonite carbonation as a possible CO2 sequestration process, Chem. Eng. Sci., 61, 4242–4251, https://doi.org/10.1016/j.ces.2006.01.048, 2006.

IPCC: Climate Change 2023: Synthesis Report. Contribution of Working Groups I, II and III to the Sixth Assessment Report of the Intergovernmental Panel on Climate Change, edited by: Lee, H. and J. Romero, , https://doi.org/10.59327/IPCC/AR6-9789291691647.001, 2023.

1010 Jiang, L.-Q., Carter, B. R., Feely, R. A., Lauvset, S. K., and Olsen, A.: Surface ocean pH and buffer capacity: past, present and future, Sci. Rep., 9, 18624, https://doi.org/10.1038/s41598-019-55039-4, 2019.

Johnson, K. S., Coale, K. H., and Jannasch, H. W.: Analytical chemistry and oceanography, Anal. Chem., 64, 1065A-1075A, https://doi.org/10.1021/ac00046a001, 1992.

Johnson, N. C., Thomas, B., Maher, K., Rosenbauer, R. J., Bird, D., and Brown, G. E.: Olivine dissolution and carbonation
1015 under conditions relevant for in situ carbon storage, Chem. Geol., 373, 93–105, https://doi.org/10.1016/j.chemgeo.2014.02.026, 2014.

Jones, D. C., Ito, T., Takano, Y., and Hsu, W.-C.: Spatial and seasonal variability of the air-sea equilibration timescale of carbon dioxide, Glob. Biogeochem. Cycles, 28, 1163–1178, https://doi.org/10.1002/2014GB004813, 2014.

Keefner, J. W., Mackwell, S. J., Kohlstedt, D. L., and Heidelbach, F.: Dependence of dislocation creep of dunite on oxygen
1020 fugacity: Implications for viscosity variations in Earth's mantle, J. Geophys. Res. Solid Earth, 116, https://doi.org/10.1029/2010JB007748, 2011.

Klein, C., Hurlbut, C. S., and Dana, J. D.: Systematic descriptions of rock-forming silicates, in: The 22nd edition of the manual of mineral science: (after James D. Dana), J. Wiley, New York, 490–563, 2002.

Köhler, P., Hartmann, J., and Wolf-Gladrow, D. A.: Geoengineering potential of artificially enhanced silicate weathering of
1025 olivine, Proc. Natl. Acad. Sci., 107, 20228–20233, https://doi.org/10.1073/pnas.1000545107, 2010.

Kremer, D., Etzold, S., Boldt, J., Blaum, P., Hahn, K. M., Wotruba, H., and Telle, R.: Geological Mapping and Characterization of Possible Primary Input Materials for the Mineral Sequestration of Carbon Dioxide in Europe, Minerals, 9, 485, https://doi.org/10.3390/min9080485, 2019.

Lackner, K. S.: Carbonate Chemistry for Sequestering Fossil Carbon, Annu. Rev. Energy Environ., 27, 193–232,
1030 https://doi.org/10.1146/annurev.energy.27.122001.083433, 2002.

Lasaga, A. C., Soler, J. M., Ganor, J., Burch, T. E., and Nagy, K. L.: Chemical weathering rate laws and global geochemical
cycles, Geochim. Cosmochim. Acta, 58, 2361–2386, https://doi.org/10.1016/0016-7037(94)90016-7, 1994.

Le Maitre, R. W., Streckeisen, A., Zanettin, B., Le Bas, M. J., Bonin, B., and Bateman, P. (Eds.): Igneous Rocks: A
Classification and Glossary of Terms: Recommendations of the International Union of Geological Sciences Subcommission
1035 on the Systematics of Igneous Rocks, 2nd ed., Cambridge University Press, Cambridge,
https://doi.org/10.1017/CBO9780511535581, 2002.

Lin, C. Y., Turchyn, A. V., Krylov, A., and Antler, G.: The microbially driven formation of siderite in salt marsh sediments,
Geobiology, 18, 207–224, https://doi.org/10.1111/gbi.12371, 2020.

Luce, R. W., Bartlett, R. W., and Parks, G. A.: Dissolution kinetics of magnesium silicates, Geochim. Cosmochim. Acta, 36,
1040 35–50, https://doi.org/10.1016/0016-7037(72)90119-6, 1972.

Lueker, T. J., Dickson, A. G., and Keeling, C. D.: Ocean pCO2 calculated from dissolved inorganic carbon, alkalinity, and
equations for K1 and K2: validation based on laboratory measurements of CO2 in gas and seawater at equilibrium, Mar. Chem.,
70, 105–119, https://doi.org/10.1016/S0304-4203(00)00022-0, 2000.

Lunstrum, A., Van Den Berghe, M., Bian, X., John, S., Nealson, K., and West, A. J.: Bacterial use of siderophores increases
1045 olivine dissolution rates by nearly an order of magnitude | Geochemical Perspectives Letters, Geochem. Perspect. Lett., 25,
https://doi.org/10.7185/geochemlet.2315, 2023.

Mackenzie, F. T. and Lerman, A.: Carbon Dioxide in Natural Waters, in: Carbon in the Geobiosphere — Earth's Outer Shell
—, edited by: Mackenzie, F. T. and Lerman, A., Springer Netherlands, Dordrecht, 123–147, https://doi.org/10.1007/1-4020-
4238-8_1, 2006.

1050 Maher, K., Johnson, N. C., Jackson, A., Lammers, L. N., Torchinsky, A. B., Weaver, K. L., Bird, D. K., and Brown, G. E.: A
spatially resolved surface kinetic model for forsterite dissolution, Geochim. Cosmochim. Acta, 174, 313–334,
https://doi.org/10.1016/j.gca.2015.11.019, 2016.

Mével, C.: Serpentinization of abyssal peridotites at mid-ocean ridges, Comptes Rendus Geosci., 335, 825–852,
https://doi.org/10.1016/j.crte.2003.08.006, 2003.

1055 Meysman, F. J. R.: Cable Bacteria Take a New Breath Using Long-Distance Electricity, Trends Microbiol., 26, 411–422,
https://doi.org/10.1016/j.tim.2017.10.011, 2018.

Meysman, F. J. R. and Montserrat, F.: Negative CO_2 emissions via enhanced silicate weathering in coastal environments,
Biol. Lett., 13, 20160905, https://doi.org/10.1098/rsbl.2016.0905, 2017.

Meysman, F. J. R., Galaktionov, O. S., Cook, P. L. M., Janssen, F., Huettel, M., and Middelburg, J. J.: Quantifying biologically
1060 and physically induced flow and tracer dynamics in permeable sediments, Biogeosciences, 4, 627–646,
https://doi.org/10.5194/bg-4-627-2007, 2007.

Meysman, F. J. R., Risgaard-Petersen, N., Malkin, S. Y., and Nielsen, L. P.: The geochemical fingerprint of microbial long-distance electron transport in the seafloor, Geochim. Cosmochim. Acta, 152, 122–142, https://doi.org/10.1016/j.gca.2014.12.014, 2015.

1065 Middelburg, J. J., Soetaert, K., and Hagens, M.: Ocean Alkalinity, Buffering and Biogeochemical Processes, Rev. Geophys., 58, e2019RG000681, https://doi.org/10.1029/2019RG000681, 2020.

Milliman, J. D. and Droxler, A. W.: Neritic and pelagic carbonate sedimentation in the marine environment: ignorance is not bliss, Geol. Rundsch., 85, 496–504, https://doi.org/10.1007/BF02369004, 1996.

Minx, J. C., Lamb, W. F., Callaghan, M. W., Fuss, S., Hilaire, J., Creutzig, F., Amann, T., Beringer, T., Garcia, W. de O.,

1070 Hartmann, J., Khanna, T., Lenzi, D., Luderer, G., Nemet, G. F., Rogelj, J., Smith, P., Vicente, J. L. V., Wilcox, J., and Dominguez, M. del M. Z.: Negative emissions—Part 1: Research landscape and synthesis, Environ. Res. Lett., 13, 063001, https://doi.org/10.1088/1748-9326/aabf9b, 2018.

Montserrat, F., Renforth, P., Hartmann, J., Leermakers, M., Knops, P., and Meysman, F. J. R.: Olivine Dissolution in Seawater: Implications for CO2 Sequestration through Enhanced Weathering in Coastal Environments, Environ. Sci. Technol., 51, 3960–

1075 3972, https://doi.org/10.1021/acs.est.6b05942, 2017.

Moosdorf, N., Renforth, P., and Hartmann, J.: Carbon Dioxide Efficiency of Terrestrial Enhanced Weathering, Environ. Sci. Technol., 48, 4809–4816, https://doi.org/10.1021/es4052022, 2014.

Moras, C. A., Bach, L. T., Cyronak, T., Joannes-Boyau, R., and Schulz, K. G.: Ocean alkalinity enhancement – avoiding runaway $CaCO_3$ precipitation during quick and hydrated lime dissolution, Biogeosciences, 19, 3537–3557,

1080 https://doi.org/10.5194/bg-19-3537-2022, 2022.

Morse, J. W. and Mackenzie, F. T.: Geochemistry of Sedimentary Carbonates, Elsevier Science, 1990.

Morse, J. W., Arvidson, R. S., and Lüttge, A.: Calcium Carbonate Formation and Dissolution, Chem. Rev., 107, 342–381, https://doi.org/10.1021/cr050358j, 2007.

Mulders, J. J. P. A. and Oelkers, Eric. H.: An experimental study of sepiolite dissolution rates and mechanisms at 25 °C,

1085 Geochim. Cosmochim. Acta, 270, 296–312, https://doi.org/10.1016/j.gca.2019.11.026, 2020.

Mulders, J. J. P. A., Harrison, A. L., Christ, J., and Oelkers, E. H.: Non-stoichiometric dissolution of sepiolite, Energy Procedia, 146, 74–80, https://doi.org/10.1016/j.egypro.2018.07.011, 2018.

NASEM: Ocean Alkalinity Enhancement, in: A Research Strategy for Ocean-based Carbon Dioxide Removal and Sequestration, National Academies Press (US), Washington (DC), https://doi.org/10.17226/26278, 2022.

1090 Neubeck, A., Duc, N. T., Bastviken, D., Crill, P., and Holm, N. G.: Formation of H2 and CH4 by weathering of olivine at temperatures between 30 and 70°C, Geochem. Trans., 12, 6, https://doi.org/10.1186/1467-4866-12-6, 2011.

Niles, P. B., Michalski, J., Ming, D. W., and Golden, D. C.: Elevated olivine weathering rates and sulfate formation at cryogenic temperatures on Mars, Nat. Commun., 8, 998, https://doi.org/10.1038/s41467-017-01227-7, 2017.

Oelkers, E. H.: An experimental study of forsterite dissolution rates as a function of temperature and aqueous Mg and Si

1095 concentrations, Chem. Geol., 175, 485–494, https://doi.org/10.1016/S0009-2541(00)00352-1, 2001a.

Oelkers, E. H.: General kinetic description of multioxide silicate mineral and glass dissolution, Geochim. Cosmochim. Acta, 65, 3703–3719, https://doi.org/10.1016/S0016-7037(01)00710-4, 2001b.

Oelkers, E. H., Declercq, J., Saldi, G. D., Gislason, S. R., and Schott, J.: Olivine dissolution rates: A critical review, Chem. Geol., 500, 1–19, https://doi.org/10.1016/j.chemgeo.2018.10.008, 2018.

1100   Olsen, A. A.: Forsterite Dissolution Kinetics: Applications and Implications for Chemical Weathering, 2007.

Olsen, A. A. and Donald Rimstidt, J.: Oxalate-promoted forsterite dissolution at low pH, Geochim. Cosmochim. Acta, 72, 1758–1766, https://doi.org/10.1016/j.gca.2007.12.026, 2008.

Olsen, A. A., Hausrath, E. M., and Rimstidt, J. D.: Forsterite dissolution rates in Mg-sulfate-rich Mars-analog brines and implications of the aqueous history of Mars, J. Geophys. Res. Planets, 120, 388–400, https://doi.org/10.1002/2014JE004664,

1105   2015.

Orlando, A., Borrini, D., and Marini, L.: Dissolution and carbonation of a serpentinite: Inferences from acid attack and high P–T experiments performed in aqueous solutions at variable salinity, Appl. Geochem., 26, 1569–1583, https://doi.org/10.1016/j.apgeochem.2011.06.023, 2011.

Palandri, J. L. and Kharaka, Y. K.: A Compilation of Rate Parameters of Water-Mineral Interaction Kinetics for Application

1110   to Geochemical Modeling, Geological survey Menlo Park California, 2004.

te Pas, E. E. E. M., Hagens, M., and Comans, R. N. J.: Assessment of the enhanced weathering potential of different silicate minerals to improve soil quality and sequester CO2, Front. Clim., 4, https://doi.org/10.3389/fclim.2022.954064, 2023.

Pfeffer, C., Larsen, S., Song, J., Dong, M., Besenbacher, F., Meyer, R. L., Kjeldsen, K. U., Schreiber, L., Gorby, Y. A., El-Naggar, M. Y., Leung, K. M., Schramm, A., Risgaard-Petersen, N., and Nielsen, L. P.: Filamentous bacteria transport electrons

1115   over centimetre distances, Nature, 491, 218–221, https://doi.org/10.1038/nature11586, 2012.

Pfeifer, K., Hensen, C., Adler, M., Wenzhfer, F., Weber, B., and Schulz, H. D.: Modeling of subsurface calcite dissolution, including the respiration and reoxidation processes of marine sediments in the region of equatorial upwelling off Gabon, Geochim. Cosmochim. Acta, 66, 4247–4259, https://doi.org/10.1016/S0016-7037(02)01073-6, 2002.

Pokrovsky, O. S. and Schott, J.: Kinetics and mechanism of forsterite dissolution at 25°C and pH from 1 to 12, Geochim.

1120   Cosmochim. Acta, 64, 3313–3325, https://doi.org/10.1016/S0016-7037(00)00434-8, 2000.

Prigiobbe, V., Costa, G., Baciocchi, R., Hänchen, M., and Mazzotti, M.: The effect of CO2 and salinity on olivine dissolution kinetics at 120°C, Chem. Eng. Sci., 64, 3510–3515, https://doi.org/10.1016/j.ces.2009.04.035, 2009.

Rao, A. M. F., Polerecky, L., Ionescu, D., Meysman, F. J. R., and de Beer, D.: The influence of pore-water advection, benthic photosynthesis, and respiration on calcium carbonate dynamics in reef sands, Limnol. Oceanogr., 57, 809–825,

1125   https://doi.org/10.4319/lo.2012.57.3.0809, 2012.

Rao, A. M. F., Malkin, S. Y., Montserrat, F., and Meysman, F. J. R.: Alkalinity production in intertidal sands intensified by lugworm bioirrigation, Estuar. Coast. Shelf Sci., 148, 36–47, https://doi.org/10.1016/j.ecss.2014.06.006, 2014.

Rau, G. H.: Electrochemical Splitting of Calcium Carbonate to Increase Solution Alkalinity: Implications for Mitigation of Carbon Dioxide and Ocean Acidity, Environ. Sci. Technol., 42, 8935–8940, https://doi.org/10.1021/es800366q, 2008.

1130 Raymo, M. E. and Ruddiman, W. F.: Tectonic forcing of late Cenozoic climate, Nature, 359, 117–122, https://doi.org/10.1038/359117a0, 1992.

Rehfeldt, T., Jacob, D. E., Carlson, R. W., and Foley, S. F.: Fe-rich Dunite Xenoliths from South African Kimberlites: Cumulates from Karoo Flood Basalts, J. Petrol., 48, 1387–1409, https://doi.org/10.1093/petrology/egm023, 2007.

Renforth, P.: The negative emission potential of alkaline materials, Nat. Commun., 10, 1401, https://doi.org/10.1038/s41467-019-09475-5, 2019.

1135

Renforth, P. and Henderson, G.: Assessing ocean alkalinity for carbon sequestration, Rev. Geophys., 55, 636–674, https://doi.org/10.1002/2016RG000533, 2017.

Renforth, P., Jenkins, B. G., and Kruger, T.: Engineering challenges of ocean liming, Energy, 60, 442–452, https://doi.org/10.1016/j.energy.2013.08.006, 2013.

1140 Riahi, K., Bertram, C., Huppmann, D., Rogelj, J., Bosetti, V., Cabardos, A.-M., Deppermann, A., Drouet, L., Frank, S., Fricko, O., Fujimori, S., Harmsen, M., Hasegawa, T., Krey, V., Luderer, G., Paroussos, L., Schaeffer, R., Weitzel, M., van der Zwaan, B., Vrontisi, Z., Longa, F. D., Després, J., Fosse, F., Fragkiadakis, K., Gusti, M., Humpenöder, F., Keramidas, K., Kishimoto, P., Kriegler, E., Meinshausen, M., Nogueira, L. P., Oshiro, K., Popp, A., Rochedo, P. R. R., Ünlü, G., van Ruijven, B., Takakura, J., Tavoni, M., van Vuuren, D., and Zakeri, B.: Cost and attainability of meeting stringent climate targets without

1145 overshoot, Nat. Clim. Change, 11, 1063–1069, https://doi.org/10.1038/s41558-021-01215-2, 2021.

Riebesell, U., Basso, D., Geilert, S., Dale, A. W., and Kreuzburg, M.: Mesocosm experiments in ocean alkalinity enhancement research, State Planet, 2-oae2023, 1–14, https://doi.org/10.5194/sp-2-oae2023-6-2023, 2023.

Rigopoulos, I., Harrison, A. L., Delimitis, A., Ioannou, I., Efstathiou, A. M., Kyratsi, T., and Oelkers, E. H.: Carbon sequestration via enhanced weathering of peridotites and basalts in seawater, Appl. Geochem., 91, 197–207,

1150 https://doi.org/10.1016/j.apgeochem.2017.11.001, 2018.

Rimstidt, J. D., Brantley, S. L., and Olsen, A. A.: Systematic review of forsterite dissolution rate data, Geochim. Cosmochim. Acta, 99, 159–178, https://doi.org/10.1016/j.gca.2012.09.019, 2012.

Robinson, S. M., Santini, K., and Moroney, J.: Wollastonite, in: Industrial minerals & rocks: commodities, markets, and uses, edited by: Kogel, J. E., Trivedi, N. C., Barker, J. M., and Krukowski, S. T., SME, Littleton, Colo., 1027–1037, 2006.

1155 Rockström, J., Gaffney, O., Rogelj, J., Meinshausen, M., Nakicenovic, N., and Schellnhuber, H. J.: A roadmap for rapid decarbonization, Science, 355, 1269–1271, https://doi.org/10.1126/science.aah3443, 2017.

Rosso, J. J. and Rimstidt, J. D.: A high resolution study of forsterite dissolution rates, Geochim. Cosmochim. Acta, 64, 797–811, https://doi.org/10.1016/S0016-7037(99)00354-3, 2000.

Saldi, G. D., Jordan, G., Schott, J., and Oelkers, E. H.: Magnesite growth rates as a function of temperature and saturation

1160 state, Geochim. Cosmochim. Acta, 73, 5646–5657, https://doi.org/10.1016/j.gca.2009.06.035, 2009.

Sanderson, B. M., O'Neill, B. C., and Tebaldi, C.: What would it take to achieve the Paris temperature targets?, Geophys. Res. Lett., 43, 7133–7142, https://doi.org/10.1002/2016GL069563, 2016.

Santos, R. M., Van Audenaerde, A., Chiang, Y. W., Iacobescu, R. I., Knops, P., and Van Gerven, T.: Nickel Extraction from Olivine: Effect of Carbonation Pre-Treatment, Metals, 5, 1620–1644, https://doi.org/10.3390/met5031620, 2015.

1165   Sarmiento, J. L. and Gruber, N.: Ocean Biogeochemical Dynamics, Princeton University Press, https://doi.org/10.2307/j.ctt3fgxqx, 2006.

Schippers, A. and Jørgensen, B. B.: Biogeochemistry of pyrite and iron sulfide oxidation in marine sediments, Geochim. Cosmochim. Acta, 66, 85–92, https://doi.org/10.1016/S0016-7037(01)00745-1, 2002.

Schuiling, R. D. and Krijgsman, P.: Enhanced Weathering: An Effective and Cheap Tool to Sequester Co2, Clim. Change, 74,

1170   349–354, https://doi.org/10.1007/s10584-005-3485-y, 2006.

Schulz, K. G., Bach, L. T., and Dickson, A. G.: Seawater carbonate chemistry considerations for ocean alkalinity enhancement research: theory, measurements, and calculations, State Planet, 2-oae2023, 1–14, https://doi.org/10.5194/sp-2-oae2023-2-2023, 2023.

Schwarzenbach, E. M., Früh-Green, G. L., Bernasconi, S. M., Alt, J. C., Shanks Iii, W. C., Gaggero, L., and Crispini, L.: Sulfur

1175   geochemistry of peridotite-hosted hydrothermal systems: Comparing the Ligurian ophiolites with oceanic serpentinites, Geochim. Cosmochim. Acta, 91, 283–305, https://doi.org/10.1016/j.gca.2012.05.021, 2012.

Sherman, G. D. and Uehara, G.: The Weathering of Olivine Basalt in Hawaii and its Pedogenic Significance, Soil Sci. Soc. Am. J., 20, 337–340, https://doi.org/10.2136/sssaj1956.03615995002000030011x, 1956.

Shirokova, L. S., Bénézeth, P., Pokrovsky, O. S., Gerard, E., Ménez, B., and Alfredsson, H.: Effect of the heterotrophic

1180   bacterium Pseudomonas reactans on olivine dissolution kinetics and implications for CO2 storage in basalts, Geochim. Cosmochim. Acta, 80, 30–50, https://doi.org/10.1016/j.gca.2011.11.046, 2012.

Siegel, D. I. and Pfannkuch, H. O.: Silicate mineral dissolution at pH 4 and near standard temperature and pressure, Geochim. Cosmochim. Acta, 48, 197–201, https://doi.org/10.1016/0016-7037(84)90362-4, 1984.

Silburn, B., Kröger, S., Parker, E. R., Sivyer, D. B., Hicks, N., Powell, C. F., Johnson, M., and Greenwood, N.: Benthic pH

1185   gradients across a range of shelf sea sediment types linked to sediment characteristics and seasonal variability, Biogeochemistry, 135, 69–88, https://doi.org/10.1007/s10533-017-0323-z, 2017.

Sissmann, O., Daval, D., Brunet, F., Guyot, F., Verlaguet, A., Pinquier, Y., Findling, N., and Martinez, I.: The deleterious effect of secondary phases on olivine carbonation yield: Insight from time-resolved aqueous-fluid sampling and FIB-TEM characterization, Chem. Geol., 357, 186–202, https://doi.org/10.1016/j.chemgeo.2013.08.031, 2013.

1190   Smith, K. L., Milnes, A. R., and Eggleton, R. A.: Weathering of Basalt: Formation of Iddingsite, Clays Clay Miner., 35, 418–428, https://doi.org/10.1346/CCMN.1987.0350602, 1987.

Smith, P., Davis, S. J., Creutzig, F., Fuss, S., Minx, J., Gabrielle, B., Kato, E., Jackson, R. B., Cowie, A., Kriegler, E., van Vuuren, D. P., Rogelj, J., Ciais, P., Milne, J., Canadell, J. G., McCollum, D., Peters, G., Andrew, R., Krey, V., Shrestha, G., Friedlingstein, P., Gasser, T., Grübler, A., Heidug, W. K., Jonas, M., Jones, C. D., Kraxner, F., Littleton, E., Lowe, J., Moreira,

1195   J. R., Nakicenovic, N., Obersteiner, M., Patwardhan, A., Rogner, M., Rubin, E., Sharifi, A., Torvanger, A., Yamagata, Y.,

Edmonds, J., and Yongsung, C.: Biophysical and economic limits to negative CO 2 emissions, Nat. Clim. Change, 6, 42–50, https://doi.org/10.1038/nclimate2870, 2016.

Strefler, J., Amann, T., Bauer, N., Kriegler, E., and Hartmann, J.: Potential and costs of carbon dioxide removal by enhanced weathering of rocks, Environ. Res. Lett., 13, 034010, https://doi.org/10.1088/1748-9326/aaa9c4, 2018.

1200 Su, B., Chen, Y., Guo, S., and Liu, J.: Origins of orogenic dunites: Petrology, geochemistry, and implications, Gondwana Res., 29, 41–59, https://doi.org/10.1016/j.gr.2015.08.001, 2016.

Summers, C. A., Dahlin, D. C., Rush, G. E., O'Connor, W. K., and Gerdemann, S. J.: Grinding methods to enhance the reactivity of olivine, Min. Metall. Explor., 22, 140–144, https://doi.org/10.1007/BF03403128, 2005.

Sun, K. H. and Huggins, M. L.: Energy additivity in oxygen-containing crystals and glasses., J. Phys. Colloid Chem., 51, 438–
1205 443, https://doi.org/10.1021/j150452a009, 1947.

Sun, M.-S.: The Nature of Iddingsite in Some Basaltic Rocks of New Mexico*, Am. Mineral., 42, 525–533, 1957.

Terlouw, T., Bauer, C., Rosa, L., and Mazzotti, M.: Life cycle assessment of carbon dioxide removal technologies: a critical review, Energy Environ. Sci., 14, 1701–1721, https://doi.org/10.1039/D0EE03757E, 2021.

Tester, J. W., Worley, W. G., Robinson, B. A., Grigsby, C. O., and Feerer, J. L.: Correlating quartz dissolution kinetics in pure
1210 water from 25 to 625°C, Geochim. Cosmochim. Acta, 58, 2407–2420, https://doi.org/10.1016/0016-7037(94)90020-5, 1994.

Torres, M. A., Dong, S., Nealson, K. H., and West, A. J.: The kinetics of siderophore-mediated olivine dissolution, Geobiology, 17, 401–416, https://doi.org/10.1111/gbi.12332, 2019.

Tosca, N. J. and Masterson, A. L.: Chemical controls on incipient Mg-silicate crystallization at 25°C: Implications for early and late diagenesis, Clay Miner., 49, 165–194, https://doi.org/10.1180/claymin.2014.049.2.03, 2014.

1215 Turchyn, A. V., Bradbury, H. J., Walker, K., and Sun, X.: Controls on the Precipitation of Carbonate Minerals Within Marine Sediments, Front. Earth Sci., 9, https://doi.org/10.3389/feart.2021.618311, 2021.

UNFCCC: Paris Agreement to the United Nations Framework Convention on Climate Change, 2015.

Van Herk, J., Pietersen, H. S., and Schuiling, R. D.: Neutralization of industrial waste acids with olivine — The dissolution of forsteritic olivine at 40–70°C, Chem. Geol., 76, 341–352, https://doi.org/10.1016/0009-2541(89)90102-2, 1989.

1220 Vandeginste, V., Lim, C., and Ji, Y.: Exploratory Review on Environmental Aspects of Enhanced Weathering as a Carbon Dioxide Removal Method, Minerals, 14, 75, https://doi.org/10.3390/min14010075, 2024.

Velbel, M. A.: Bond strength and the relative weathering rates of simple orthosilicates, Am. J. Sci., 299, 679–696, https://doi.org/10.2475/ajs.299.7-9.679, 1999.

Velbel, M. A.: Dissolution of olivine during natural weathering, Geochim. Cosmochim. Acta, 73, 6098–6113,
1225 https://doi.org/10.1016/j.gca.2009.07.024, 2009.

Vesta: North Sea Beach Annual Monitoring Report, 2023.

Wallmann, K., Aloisi, G., Haeckel, M., Tishchenko, P., Pavlova, G., Greinert, J., Kutterolf, S., and Eisenhauer, A.: Silicate weathering in anoxic marine sediments, Geochim. Cosmochim. Acta, 72, 2895–2918, https://doi.org/10.1016/j.gca.2008.03.026, 2008.

1230   Wang, B., Gao, X., Song, J., Li, X., Yuan, H., Xie, L., Zhao, J., Xing, Q., and Qin, S.: Feasibility of increasing marine carbon storage through olivine addition, J. Environ. Chem. Eng., 11, 111221, https://doi.org/10.1016/j.jece.2023.111221, 2023.

White, A. F. and Brantley, S. L. (Eds.): Chemical Weathering Rates of Silicate Minerals, De Gruyter, Berlin, Boston, https://doi.org/doi:10.1515/9781501509650, 1995.

Widdicombe, S., Spicer, J. I., and Kitidis, V.: Effects of ocean acidification on sediment fauna, in: Ocean Acidification, edited

1235   by: Gattuso, J.-P., Hansson, L., Gattuso, J.-P., and Hansson, L., Oxford University Press, Oxford, New York, 2011.

Wilshire, H. G.: Alteration of olivine and orthopyroxene in basic lavas and shallow intrusions, Am. Mineral., 43, 120–147, 1958.

Wilson, M. J.: Weathering of the primary rock-forming minerals: processes, products and rates, Clay Miner., 39, 233–266, https://doi.org/10.1180/0009855043930133, 2004.

1240   Wogelius, R. A. and Walther, J. V.: Olivine dissolution at 25°C: Effects of pH, CO2, and organic acids, Geochim. Cosmochim. Acta, 55, 943–954, https://doi.org/10.1016/0016-7037(91)90153-V, 1991.

Wolf-Gladrow, D. A., Zeebe, R. E., Klaas, C., Körtzinger, A., and Dickson, A. G.: Total alkalinity: The explicit conservative expression and its application to biogeochemical processes, Mar. Chem., 106, 287–300, https://doi.org/10.1016/j.marchem.2007.01.006, 2007.

1245   Wollast, R., Mackenzie, F. T., and Bricker, O. P.: Experimental precipitation and genesis of sepiolite at earth-surface conditions, Am. Mineral., 53, 1645–1662, 1968.

Xu, Y.-Y., Pierrot, D., and Cai, W.-J.: Ocean carbonate system computation for anoxic waters using an updated CO2SYS program, Mar. Chem., 195, 90–93, https://doi.org/10.1016/j.marchem.2017.07.002, 2017.

Zeebe, R. E. and Wolf-Gladrow, D. (Eds.): Chapter 1 Equilibrium, in: Elsevier Oceanography Series, vol. 65, Elsevier, 1–84,

1250   https://doi.org/10.1016/S0422-9894(01)80002-7, 2001.

Zhu, Q., Aller, R. C., and Fan, Y.: Two-dimensional pH distributions and dynamics in bioturbated marine sediments, Geochim. Cosmochim. Acta, 70, 4933–4949, https://doi.org/10.1016/j.gca.2006.07.033, 2006.